



## Air-parcel residence times in a mature forest: observational evidence from a free-air CO<sub>2</sub> enrichment experiment

Edward J. Bannister<sup>1,3</sup>, Mike Jesson<sup>2,1</sup>, Nicholas J. Harper<sup>1</sup>, Kris M. Hart<sup>1</sup>, Giulio Curioni<sup>1</sup>, Xiaoming Cai<sup>4,3</sup>, A. Rob MacKenzie<sup>1,3</sup>

<sup>1</sup> Birmingham Institute of Forest Research, University of Birmingham, Edgbaston, Birmingham, United Kingdom

<sup>2</sup> Department of Civil Engineering, University of Birmingham, Edgbaston, Birmingham, United Kingdom

<sup>3</sup> Department of Geography, Earth, and Environmental Sciences, University of Birmingham, Edgbaston, Birmingham, United Kingdom

<sup>4</sup> Retired

Correspondence to: Rob MacKenzie (a.r.mackenzie@bham.ac.uk)

**Abstract.** In forests, air-parcel residence times—the inverse of first-order exchange rates—influence in-canopy chemistry and the exchanges of momentum, energy, and mass with the surrounding atmosphere. Accurate estimates are needed for chemical investigations of reactive trace species, such as volatile organic compounds, some of whose chemical lifetimes are in the order of average residence times. However, very few observational residence-time estimates have been reported. Little is known about even the basic statistics of real-world residence times or how they are influenced by meteorological variables such as turbulence or atmospheric stability. Here, we report opportunistic investigations of air-parcel residence times in a free-air carbon dioxide enrichment (FACE) facility in a mature, broadleaf deciduous forest with canopy height  $h_c \approx 25$  m. Using nearly 50 million FACE observations, we find that median daytime residence times in the tree crowns range from around 70 s when the trees are in leaf to just over 34 s when they are not. Air-parcel residence times increase with increasing atmospheric stability, as does the dispersion around their central value. Residence times scale approximately with the reciprocal of the friction velocity,  $u_*$ . During some calm evenings in the growing season, we observe distinctly different behaviour: pooled air being sporadically and unpredictably vented—evidenced by sustained increases in CO<sub>2</sub> concentration—when intermittent turbulence penetrates the canopy. In these conditions, the concept of a residence time is less clearly defined. Parameterisations available in the literature underestimate turbulent exchange in the upper half of forest crowns and overestimate the frequency of long residence times. Robust parameterisations of air-parcel residence times (or, equivalently, fractions of emissions escaping the canopy) may be generated from inverse gamma distributions, with the parameters  $1.4 \leq \alpha \leq 1.8$  and  $\beta = h_c/u_*$  estimated from widely measured flow variables. In this case, the mean value for  $\tau$  becomes formally defined as  $\bar{\tau} = \beta/(\alpha - 1)$ . For species released in the canopy during the daytime, chemical transformations are unlikely unless the reaction time scale is in the order of a few minutes or less.

### 1 Introduction

Forests cover nearly a third of the Earth's land surface and exchange momentum, energy, and mass with the atmosphere. Forest-atmosphere exchanges are fundamental to forest ecology, involving transfers of water vapour, carbon dioxide (CO<sub>2</sub>), trace gases including biogenic volatile organic compounds (BVOCs), and particles such as pollen and spores. Forest-atmosphere exchanges also influence air quality, meteorology, and the climate, for example, through BVOCs interacting with oxidants such as O<sub>3</sub> and OH (Fuentes et al., 2000; MacKenzie et al., 2011; Peñuelas and Staudt, 2010; Pyle et al., 2011; Rap et al., 2018).

Turbulent motions transport the air from the boundary layers around the forest elements into the canopy airspace and out into the surrounding atmosphere. The properties of these turbulent motions depend on factors such as a forest's structure and the



atmospheric conditions (Bannister et al., 2022; Brunet, 2020; Finnigan, 2000). The turbulent exchange determines the extent to which a forest is ventilated, i.e., how quickly the air within the forest is replaced by air from the surroundings. The rate at which a forest is ventilated is especially pertinent when considering reactive compounds, such as many BVOCs, whose chemical lifetimes can be in the order of a few minutes (Kesselmeier and Staudt, 1999). In this context, it is helpful to consider a ‘residence time’, which refers to a representative amount of time air parcels spend within the forest air space. During this time, the air parcels can exchange mass with the forest and one another, and the gases within them may participate in chemical reactions. Accurate estimates of air-parcel residence times in forests are needed to scale leaf-level chemistry and meteorology to the regional and global scales relevant to commerce and policy (Forkel et al., 2015; Guenther et al., 2012). Residence times and other time-scale estimates are commonly used in urban studies, for example, to quantify how well a city is ventilated, or the time over which pedestrians are exposed to pollutants (e.g., Cai, 2012; Lau et al., 2020; Lin et al., 2014; Lo and Ngan, 2017).

There is no single definition of an air-parcel residence time in forests, although a Lagrangian approach probably offers the simplest conceptual picture. For example, one can imagine an air parcel passing over a source of a BVOC, such as a sunlit leaf, then passing through the forest air space, and eventually leaving the forest. Tracking the trajectories of lots of air parcels in this way allows one to derive a statistical residence time. The first attempts to investigate the statistics of air parcels in forests adopted a Lagrangian stochastic (LS) approach to exploit this basic idea (Fuentes et al., 2007; Strong et al., 2004). These LS modelling studies suggest that air-parcel residence times depend strongly on the parcel’s release height. The mean residence times range from a few seconds, for parcels travelling from the forest crown, to several minutes for parcels travelling from near the forest floor (Fuentes et al., 2007; Strong et al., 2004). Long residence times—ten minutes or more—have been calculated to occur almost exclusively for parcels travelling from the lower third of the canopy.

Gerken et al. (2017) (hereafter GCF17) offer the most complete statistical account of air-parcel residence times in forests. GCF17 propose an elegant model for the distribution of residence times by adapting the inverse-Gaussian distribution and representing turbulent transport using eddy-diffusivity closure. The residence times,  $\tau$ , have a probability density function (PDF) given by the distribution of first passage through a plane at  $z = h_c$ , where  $h_c$  is the mean height of the forest. For a given release height,  $z_{rel}$ , the PDF is

$$p(\tau; z_{rel}) = \frac{|h_c - z_{rel}|}{\sqrt{4\pi K_{eq}}} \tau^{-\frac{3}{2}} \exp\left[-\frac{(h_c - z_{rel})^2}{4K_{eq}\tau}\right], \quad (1)$$

where  $K_{eq}$  is a constant eddy diffusivity at each  $z_{rel}$  (but may differ for different  $z_{rel}$ ). GCF17 use Eq. (1) to define turbulent transport time scale

$$\tau_{turb}(z_{rel}) = \frac{(h_c - z_{rel})^2}{4K_{eq}(z_{rel})}. \quad (2)$$

Equation (1) predicts an exponential increase in probability with increasing  $\tau$ , followed by a heavy-tailed  $\tau^{-3/2}$  power-law decrease beyond the mode (i.e., as  $\tau$  becomes large relative to  $\tau_{turb}$ , the exponential term approaches unity). In forests and other plant canopies, eddy-diffusivity closure is imperfect and may be unsuitable for certain applications (Bannister et al., 2022; Finnigan, 2000; Monteith and Unsworth, 2008). However, it remains widely adopted in larger scale models because it allows in-canopy turbulent transfer to be estimated from a modest number of variables, without the prohibitive computational expense of more sophisticated closure schemes. GCF17 acknowledge the limitations of eddy-diffusivity closure and find support for Eq. (1) in that it agreed quite well with results obtained using large-eddy simulations (LES) of idealised forest canopies, particularly for parcels travelling from low down in the canopy (LES does not rely on the same closure assumptions as Eq. (1)).



80

GCF17 find that the median values of  $\tau$  range from a few seconds in the upper crowns to around 30 minutes near the forest floor, with the dispersion in  $\tau$  decreasing rapidly with height. GCF17 also showed that the density and morphology of vegetation influences air-parcel residence times. The values of  $\tau$  values increase with the leaf area index (LAI)—the ratio of total projected leaf area per unit ground area—other than for parcels released high in the canopy. Bailey et al. (2014) obtained  
85 similar results in LES investigations of exchange around short, trellis-trained crops. Bailey et al. (2014) also found residence times were longer in homogeneous canopies than heterogeneous ones. In an LES investigation of flow over forested hills, residence times of Lagrangian air parcels emitted in the lower part of the canopy were shorter than those moving over flat terrain (Chen et al., 2019).

90 Researchers have also used Eulerian frameworks to investigate residence times in forests. Edburg et al. (2012) use LES to calculate mean residence times of 8.6, 3.6, and 5.6 min for ground, canopy, and mixed sources of passive scalars released in a homogeneous forest, within the range of reported values using LS models. Wolfe et al. (2011) use a simple canopy resistance model to estimate air-parcel residence times of around 2 min for a ponderosa pine plantation.

95 Because of the challenges in calculating air-parcel residence times from point observations, field estimates are rarely reported, meaning there is little data against which modelling estimates can be tested. A handful of studies have used  $^{222}\text{Rn}$ , a radioactive gas produced along the  $\alpha$ -decay chains of uranium, as an inert tracer. Because  $^{222}\text{Rn}$  is inert and originates in the soil, provided the ground flux is known, its concentration in the forest airspace can be used to infer a canopy ventilation rate (Martens et al., 2004; Simon et al., 2005; Trumbore et al., 1990). Trumbore et al. (1990) used  $^{222}\text{Rn}$  measurements to calculate mean canopy  
100 residence times of  $\leq 1$  h and 3.4–5.5 h for day- and night-time conditions, respectively, in a mature Amazon Rainforest site ( $h_c \approx 30$  m). Subsequent measurements at other Amazonian locations have reported mean residence times ranging from around a minute during the day to several hours at night (Martens et al., 2004; Rummel, 2005; Simon et al., 2005). Measurements in a young ponderosa pine plantation ( $h_c = 5.7$  m) in California, USA found daytime summer residence times ranging from 70–420s (Farmer and Cohen, 2008). It is possible to estimate residence times through indirect methods, such as  
105 calculating the mean time between scalar ramps in the ejection–sweep cycle that dominates turbulent exchange between forests and the atmosphere (Katul et al., 1996; Paw U et al., 1995; Rummel et al., 2002). These methods have been used to estimate air-parcel residence times of a minute or two during the day to around an hour at night (Rummel et al., 2002). However, there are no field reports of air-parcel residence time statistics beyond their mean values, which provide limited information in, for example, calculating the probability of a BVOC reacting during its passage out of a forest. Further, little is known about the  
110 influence of even basic meteorological variables on air-parcel residence times in forests.

Here, we report opportunistic investigations of air-parcel residence times in the mature, broadleaf deciduous forest at the Birmingham Institute of Forest Research (BIFoR) free-air carbon dioxide enrichment (FACE) facility. The primary experiment at BIFoR FACE observes forest ecosystem behaviour under future atmospheric composition. This is achieved by using large-  
115 scale infrastructure to elevate the  $\text{CO}_2$  mixing ratio, without containment, to  $150 \mu\text{mol mol}^{-1}$  above ambient in several large patches of the forest (Hart et al., 2020; MacKenzie et al., 2021). BIFoR FACE is one of two ‘second-generation’ FACE experiments on mature, ecosystem-scale forests, the other being the ‘EucFACE’ experiment in an open sclerophyll forest in Australia (Drake et al., 2016). If we focus our attention on time scales of seconds to hours, over which the  $\text{CO}_2$  is approximately passive, the normal course of operation of BIFoR FACE also offers a unique, daily dispersal experiment. Across several  
120 patches of the mature woodland, the  $\text{CO}_2$  mixing ratio is elevated around sunrise, held at  $150 \mu\text{mol mol}^{-1}$  above ambient during daylight hours, and allowed to return to ambient after sunset, when the  $\text{CO}_2$  release is stopped. We use three years’ data (just



under 50 million observations) to investigate the effect of canopy structure and the surrounding atmospheric conditions on air-parcel residence times in a mature temperate forest.

## 2 Methods

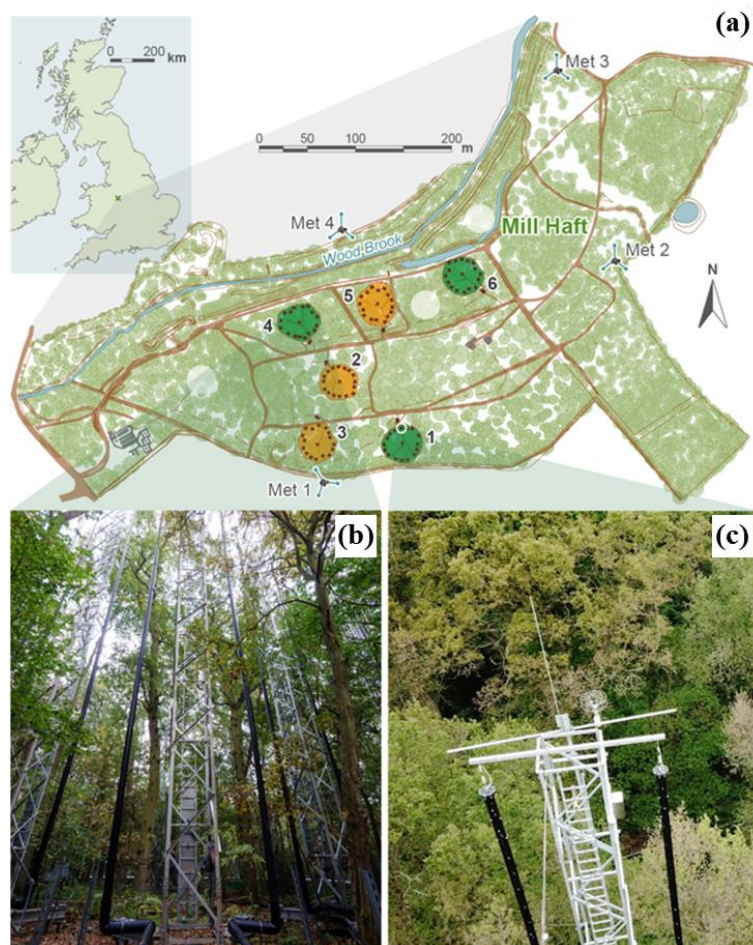
### 125 2.1 Site description

The BIFoR FACE facility is located in a mature deciduous broadleaf forest patch ( $\approx 19$  ha) in central England, United Kingdom (latitude, longitude: 52.7996, -2.3039). The BIFoR FACE woodland is dominated by *Quercus robur* (pedunculate oak), with a dense heterogeneous understorey layer of *Corylus avellana* (hazel), *Crataegus monogyna* (common hawthorn), *Acer pseudoplanatus* (sycamore), and *Ilex aquifolium* (holly). Below the heterogeneous understorey, the woodland supports ground  
130 flora, including *Phegopteris connectilis* (beech fern), *Rubus fruticosus* (bramble), *Hedera spp.* (ivy), *Lonicera periclymenum* (honeysuckle), and, where the canopy has been opened for access rides, various grass species (G. Platt, private communication, 2019). The BIFoR FACE woodland shows evidence of historical coppicing but it has not been managed for at least 30 years. The largest oaks were planted in 1850. Hanging and fallen deadwood is left in place except where it poses a direct risk to human safety. The highest point of the facility is situated in the east of the forest, at around +112 m above sea level (a.s.l.) and  
135 the lowest point at the site offices and CO<sub>2</sub> storage plant, at +92 m a.s.l. The terrain below the areas of experimental interest is quite level, at +108  $\pm$  2.7 m a.s.l. (see contour maps in MacKenzie et al. (2021)).

The BIFoR FACE facility comprises nine experimental patches of forest, which are approximately circular, with an internal radius of around 17 m (Table 1). There are three ‘fumigated’ (f) patches, in which infrastructure arrays maintain the CO<sub>2</sub>  
140 mixing ratio (denoted [CO<sub>2</sub>] hereafter) at 150  $\mu\text{mol mol}^{-1}$  above ambient during daylight periods of the growing season. There are three further ‘control’ (c) patches, which are dosed with ambient air only, and three ‘ghost’ patches, which are ecologically similar to the fumigated and control patches, but do not contain any of the supporting infrastructure (Figure 1). In the fumigated arrays, premixed air/CO<sub>2</sub> is released in the upwind quadrant from perforated vent pipes, supported by 16 free-standing lattice towers (Figure 1). The wind direction and speed are updated in the FACE control program (FCP) every second, based on 20 Hz  
145 sonic anemometer measurements at the canopy top on the northernmost tower of each fumigated array (Hart et al., 2020). The forest arrays are paired, so that a control array mimics the actions of its corresponding fumigated array, but doses the forest patch with ambient air only. The pairings are numbered 1(f) and 3(c), 4(f) and 2(c), 6(f) and 5(c) (Figure 1). For more background on the BIFoR FACE facility and its operation, see Hart et al. (2020). Details of the measurements and data and tissue curation pipelines are provided in MacKenzie et al. (2021).

150 **Table 1: Geometries of the BIFoR FACE control (c) and fumigation (f) arrays. The internal radius is defined as the mean distance between the central tower and the inside edge of the towers supporting the perforated vent pipes.**

Array	Infrastructure tower heights (m)	Central tower height (m)	Height of CO <sub>2</sub> sample inlet	Internal radius (m)	Research ground area (m <sup>2</sup> )	Array volume (m <sup>3</sup> )
1(f)	26.7	26.0	21.5	17	724	24,815
2(c)	25.6	24.9	22.5	16	628	21,107
3(c)	26.2	25.5	21	16	661	22,138
4(f)	27.2	26.5	22	17	702	24,406
5(c)	27.3	26.6	22.5	17	688	24,207
6(f)	24.7	24.0	19.8	17	678	21,641



155 **Figure 1:** (a) schematic of the BIFoR FACE facility. The coloured circles indicate the location of the FACE arrays, with green and orange denoting the fumigated and control arrays, respectively. The grey translucent circles mark the locations of the ghost arrays. The meteorological towers on the edge of the forest are labelled Met 1–4. (b) The perforated FACE vent pipes in array 4. (c) The two-dimensional sonic anemometer in array 1. Figure 1a © Crown copyright and database rights 2021. Ordnance Survey (100025252).

## 2.2 Observational details

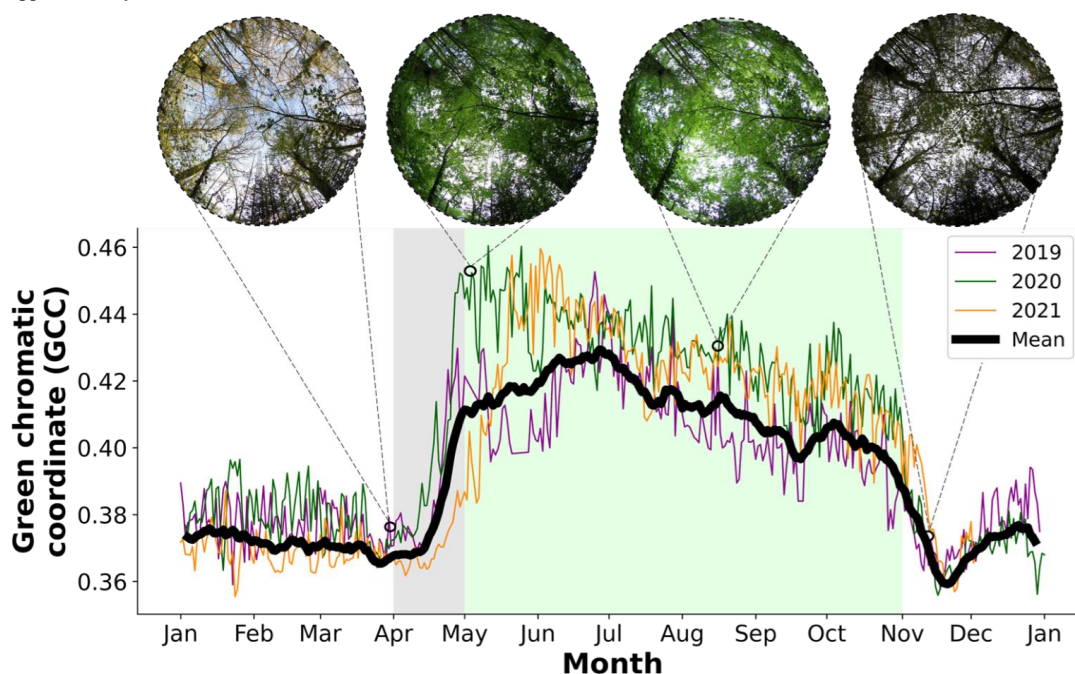
### 160 2.2.1 Observation period and canopy density

The FACE arrays operate up to 18 hours a day (04:30–21:30), depending on day length, and from budburst (around 1 April) to leaf fall (around 31 October). We investigate observations from 1 April–31 October in the years 2019–2021. We refer to the April fumigation period as ‘leaf-off’, because the dominant canopy oaks put out most of their leaves in May, and the period from 1 May to 31 October as ‘leaf-on’. Together the leaf-on and leaf-off periods, as defined, make up the CO<sub>2</sub> fumigation period at BIFoR FACE. The LAI is much greater during the leaf-on period than the leaf-off period—see, for example, the hemispheric photographs in Figure 2. The LAI  $\approx$  7–8 during the leaf-on period, calculated using extensive leaf-litter measurements throughout the season. The plant area index (PAI)—the total projected plant area per unit ground area—is approximately 1–2 for the leaf-off period, however, this is only a rough estimate. Deriving PAI estimates from digital photographs, for example, is problematic in tall multi-layered forests (Yan et al., 2019) and leaf litter observations are not available. To show the broad phenological changes at BIFoR FACE, Figure 2 presents timeseries of the green chromatic coordinate (GCC) for the investigation period. The GCC (normalised to take values from 0–1) measures the ‘greenness’ of the

165  
170



canopy from repeated digital photographs (Woebbecke et al., 1995). Figure 2 shows that the greenness of BIFoR FACE forest increases sharply towards the end of April, as the canopy oaks begin to put out their leaves, peaks in May–June, declines slowly across the leaf-on period as the leaves mature, before declining sharply in November when the dominant oaks drop their leaves. A note of caution: although the GCC is a helpful tool to monitor seasonal canopy-scale dynamics (Toomey et al., 2015), it is not a proxy for plant-area density in multi-layered deciduous forests. For example, in Figure 2, the sharp changes in GCC in spring and autumn correspond to changes in leaf density, but the gentle decrease in GCC over the leaf-on period is not reflected by changes in canopy density (i.e., the leaves become less green over the summer, but their number remains approximately constant).



180

**Figure 2:** Timeseries of the green chromatic coordinate (GCC) derived from PhenoCam measurements. The hemispheric photos are taken by cameras around 50 cm above the ground in array 1. Shaded grey and green regions show the leaf-off and leaf-on periods, respectively.

### 185 2.2.2 Fumigation and meteorological measurements

The FCP determines, based on solar elevation, the times at which the fumigation is started and shut down each day. Array pairings are switched on in sequence 1(f) + 3(c), 2(c) + 4(f) and 5(c) + 6(f). Wind velocities for the FCP are monitored at 1 Hz using two-dimensional sonic anemometers (WMT700, Vaisala Oyj, Vantaa, Finland), mounted at a height  $z \approx 1$  m above the canopy on the northernmost tower of each fumigated array. The FCP logs 1-min averages of the wind speed and direction, and of other variables including the air temperature, atmospheric pressure, and solar elevation. There are four meteorological masts around the edge of the forest (denoted Met 1–4, respectively; Figure 1), with three-dimensional sonic anemometers (R3-100, Gill Instruments, Lymington, UK) mounted at 25 m on each. These anemometers sampled the three-dimensional instantaneous velocity components and the speed of sound at 20 Hz throughout the entire observational period. In October 2020, three additional three-dimensional sonic anemometers (Windmaster Pro, Gill Instruments, Lymington, UK) were added to each mast at heights of 7 m, 10 m, and 14 m, sampling the same variables at the same rate as the existing sensors. The  $[\text{CO}_2]$  is measured at 1 Hz using infrared gas analysers (IRGA, LiCor 840A, LiCor Lincoln) with inlets situated in the centre of the fumigation and control arrays, just below the top of the canopy for each array (Table 1).

190

195



The FCP automatically records 1-min and 5-min averages of the 1 Hz [CO<sub>2</sub>] observations. The software halts fumigation when the canopy-top 1-min average air temperature is <4°C because broadleaf forests uptake little carbon below this threshold (Larcher, 1995). Fumigation is also stopped during periods of high winds—where the 15-min average wind speed,  $V$ , at the canopy top exceeds 8 m s<sup>-1</sup>—because of the high cost of maintaining the elevated [CO<sub>2</sub>]. When  $V < 0.4$  m s<sup>-1</sup>, the FCP introduces CO<sub>2</sub>-enriched air all around the array via alternate vent pipes, rather than in the upwind quadrant, as under normal wind speeds. This is because advection of the enriched gas flow is ineffective at very low wind speeds.

### 2.3 Calculation of residence times

We calculate residence times from the FACE data using a mass balance approach. We treat each fumigated array as a reservoir of ‘additional’ CO<sub>2</sub>, i.e., as a reservoir of air with a CO<sub>2</sub> mixing ratio that is elevated ( $e[\text{CO}_2]$ ) compared to the ambient CO<sub>2</sub> mixing ratio,  $a[\text{CO}_2]$ . The residence time represents the average time each additional molecule of CO<sub>2</sub> spends in the fumigated arrays before it is transported out by turbulent and advective fluxes, or is taken up by the trees and other plants. Provided we choose a time period over which the mass of the additional CO<sub>2</sub> in each fumigated array is approximately steady, the residence time can be interpreted equivalently as the time it would take to increase the CO<sub>2</sub> mixing ratio from  $a[\text{CO}_2]$  to  $e[\text{CO}_2]$  in the absence of significant sinks. First, we find the mixing ratio of the additional CO<sub>2</sub> in each fumigated array ( $\chi_{e\text{CO}_2}$ ) during fumigation, i.e., the difference between the elevated and ambient mixing ratios:

$$\chi_{e\text{CO}_2} (\mu\text{mol mol}^{-1}) = e[\text{CO}_2] - a[\text{CO}_2]. \quad (3)$$

The value of  $\chi_{e\text{CO}_2}$  is then used together with the ideal gas equation to calculate the mass of additional CO<sub>2</sub> in each fumigated array during fumigation:

$$M_{\text{CO}_2} = V_a M_r \chi_{e\text{CO}_2} \frac{p}{\mathcal{R}T}, \quad (4)$$

where  $M_{\text{CO}_2}$  (g) is the mass of the additional CO<sub>2</sub>,  $V_a$  (m<sup>3</sup>) is the effective volume of each fumigated array (Table 1),  $M_r$  is the molar mass of CO<sub>2</sub> (g mol<sup>-1</sup>),  $p$  is the atmospheric pressure (Pa),  $\mathcal{R}$  is the molar gas constant (8.314 m<sup>3</sup> Pa K<sup>-1</sup> mol<sup>-1</sup>), and  $T$  is the air temperature (K). For the residence time analysis across the entire study period, we treat  $V_a$  as constant for each array. However, when examining individual events such as venting in stable atmospheric conditions (section 3.7), this assumption is called into question. We define a residence time by dividing the mass of additional CO<sub>2</sub> in each array by the flow rate required to sustain it:

$$\tau = M_{\text{CO}_2} / F_{\text{in}}, \quad (5)$$

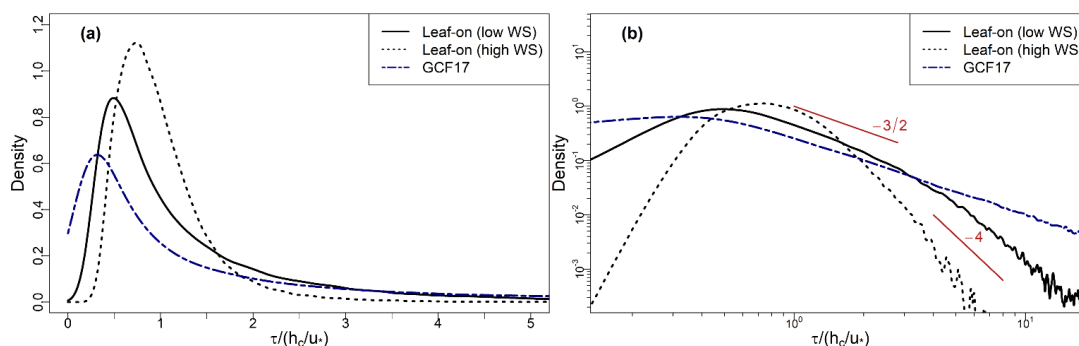
where  $\tau$  (s) is the residence time and  $F_{\text{in}}$  (g (CO<sub>2</sub>) s<sup>-1</sup>) is the CO<sub>2</sub> flow rate into each fumigated array from the FACE infrastructure. Eq. (5) discounts other sources of additional CO<sub>2</sub> into each fumigated array, most notably the soil fluxes ( $F_{\text{soil}}$ ). This is justified because  $F_{\text{in}} \gg F_{\text{soil}}$  during fumigation— $F_{\text{in}} \approx 50$ –550 g (CO<sub>2</sub>) s<sup>-1</sup> in each array, compared with  $F_{\text{soil}} < 0.1$  g (CO<sub>2</sub>) s<sup>-1</sup> (Von Arnold et al., 2005).

We consider the conditions under which Eq. (5) offers a reasonable estimate of residence times. In a quasi-infinite model of a uniform forest, such as in GCF17, the only path for air parcels to leave the canopy is through vertical venting out of the top, which we denote  $F_{\text{out}(top)}$ . The BIFoR FACE arrays, however, are not closed at the sides, and air parcels can also exit the arrays horizontally, i.e., there is some non-zero horizontal flux,  $F_{\text{out}(hor)}$ , of air out of the array. In a quasi-infinite, uniform forest, we expect  $\tau = M_{\text{CO}_2} / F_{\text{in}} \approx M_{\text{CO}_2} / F_{\text{out}(top)}$ . In reality, however,  $\tau = M_{\text{CO}_2} / F_{\text{in}} = M_{\text{CO}_2} / (F_{\text{out}(top)} + F_{\text{out}(hor)} + F_{\text{out}(sink)})$ , where  $F_{\text{out}(sink)}$  denotes CO<sub>2</sub> sink terms, most notably photosynthetic uptake. We do not include  $F_{\text{out}(sink)}$  in our calculations below because  $F_{\text{out}(sink)} \approx 0.5$ –2 g (CO<sub>2</sub>) s<sup>-1</sup> during the day (Gardner et al., 2021), typically less than 1% of the



total flux. Long-term analysis of the BIFoR FACE observations shows contamination events between the arrays are rare and  
 235 mostly small (Hart et al., 2020), usually occurring in strong winds. This suggests that, although  $F_{out(hor)}$  is always non-zero,  
 it is likely small in conditions with weak advection. Unfortunately, horizontal fluxes in forests are difficult to measure or even  
 estimate (Aubinet et al., 2010). Therefore, rather than trying to assign a numerical value to  $F_{out(hor)}$ , we identify  
 meteorological conditions under which  $F_{out(top)} \gg F_{out(hor)}$ , and therefore  $\tau = M_{CO_2}/F_{in} \approx M_{CO_2}/F_{out(top)}$ . Figure 3  
 240 presents probability density functions of  $\tau$  during the lowest 50% of wind speeds of the leaf-on period (solid black), during the  
 highest 25% of wind speeds of the leaf-on period (dashed), and GCF17's model in Eq. (1) (navy). The PDF for GCF17 takes  
 $K_{eq} = 1.2 \text{ m}^2 \text{ s}^{-1}$ , calculated using Eqs. (A1–3) in Appendix A,  $h_c = 25 \text{ m}$ , and  $z_{rel} = 15 \text{ m}$ , which reflects that the majority  
 of the  $CO_2$  is released in the upper two-thirds of the canopy (see section 2.4 below).

Figure 3 shows, at low wind speeds, our method generates PDFs of  $\tau$  in reasonably close agreement to GCF17, especially  
 245 given the very different assumptions used to calculate each PDF. Under these conditions, the one notable deviation between  
 our results and GCF17's theory is in the right tails of the PDFs (Figure 3b), which we discuss further in section 3.6. In the  
 strongest winds, however, the limited diameters of the BIFoR FACE arrays constrains our method. In these conditions, the  
 mostly small values of  $\tau$ —visible in the sharp peak of the PDF in Figure 3a and steep decay of the right tail in Figure 3b—  
 indicate that  $F_{in}$  has increased, and therefore the flux out has increased. Comparisons with GCF17 suggest this is  
 250 predominantly due to an increase in the horizontal component  $F_{out(hor)}$ , which is difficult to approximate in our finite-size  
 arrays. Our residence-time calculations below therefore include only observations during the lower half of wind speeds  
 (varying the percentile cut-off between 40–60% does not qualitatively affect our results). We discuss the implications of  
 stronger winds on  $\tau$  in sections 3.3 and 3.6.



255 **Figure 3:** (a) Linear- and (b) logarithmic-scale PDFs of  $\tau$  from BIFoR FACE during the lowest 50% (solid black) and highest 25%  
 (black dashed) of wind speeds of the leaf-on period, and GCF17's model in Eq. (1) (navy-blue dot-dash). In (b), slopes of  $-3/2$  and  $-4$   
 are shown for reference. Values of  $\tau$  normalised by  $h_c/u_*$ .

## 2.4 Data processing

We use a 5-min averaging period for the residence time calculations in Equations (3–5) and Reynolds averaging of the  
 260 meteorological tower observations below. Sensitivity testing on high-resolution velocity measurements showed this to be the  
 most appropriate period to capture the significant turbulent structures at this structurally heterogeneous site, while being long  
 enough so that  $\chi_{CO_2}$  and  $F_{in}$  were approximately steady. In mature forests, whose largest eddies scale with the mean height of  
 the canopy  $h_c$  (Bannister et al., 2022; Finnigan, 2000; Raupach et al., 1996), the canopy turnover time  $\tau_c \approx h_c/u_* \approx 30\text{--}90 \text{ s}$ ,  
 where  $u_*$  is the friction velocity measured at  $z = h_c$  (its derivation is described in section 2.4 below). This averaging period  
 265 therefore corresponds to 5–10 cycles of the dominant turbulent eddies and the statistics of the residence time calculations were  
 not qualitatively altered using averaging periods of up to 1 hr.



We discarded observations for dates on which at least one of the fumigation arrays was switched off for more than two hours, or switched on and off more than once during the normal fumigation period. These temporary shutdowns were usually for maintenance work, or during periods of exceptionally high winds (which we discarded in any case according to section 2.3). This cautious filtering threshold ensures the residence time calculations focus on periods during which the fumigation was steady, rather than when the FACE infrastructure was operating at high flow rates to increase the  $[\text{CO}_2]$  following shutdown. We also discarded dates on which observations were available from neither Met 1 nor Met 4 (see Figure 1). The filtering process left 530 observation days (78 in leaf-off and 452 in leaf-on) from a total of 642 (90 in leaf-off and 552 in leaf-on). To avoid erroneous values of  $\tau$ , we discarded entries where: (i)  $F_{in} < 1 \text{ g} (\text{CO}_2) \text{ s}^{-1}$ ; and (ii) values of  $M_{\text{CO}_2}$  lay outside the range  $\overline{M_{\text{CO}_2}} \pm 4\sigma(M_{\text{CO}_2})$ , where  $\sigma$  is the standard deviation and the overbar denotes the mean. Steps (i) and (ii) together discarded less than 0.3% of the data.

To aid comparisons with previous reports, we highlight two particular features of the fumigation at BIFoR FACE. First, the fumigation is only carried out when the trees are likely to be photosynthesising, i.e., during the daytime (with an hour or so of fumigation either side of sunrise and sunset) of the UK growing season, which is taken as 1 April–31 October. We therefore emphasise our estimates here are of forest air-parcel residence times during the daytime of the northern temperate spring, summer, and autumn. Second, most of the  $e[\text{CO}_2]$  air at BIFoR FACE is released into the oak canopy—comprising approximately the upper two-thirds of the mean forest height—where the bulk of the photosynthesising leaves are located.

## 2.5 Notation and meteorological tower calculations

We use right-handed Cartesian coordinates throughout this paper. We denote  $\mathbf{x} = (x, y, z)$ , the velocity components  $u, v, w$  (using the meteorological convention that positive  $u$  and  $v$  values indicate westerly and southerly flow, respectively), and time as  $t$ . For a quantity  $\phi(\mathbf{x}, t)$ , a double overbar denotes the time average and the prime denotes the deviations from that average, which we refer to as the ‘turbulent quantities’, i.e.  $\phi(\mathbf{x}, t) = \overline{\phi}(\mathbf{x}) + \phi'(\mathbf{x}, t)$ . The double overbar is used instead of the conventional single overbar to distinguish the time averages from the descriptive statistics elsewhere in the paper. The turbulence kinetic energy (TKE) per unit mass =  $\frac{1}{2}(\overline{u'^2} + \overline{v'^2} + \overline{w'^2})$ . The friction velocity  $u_* = \left(\overline{u'w'^2} + \overline{v'w'^2}\right)^{\frac{1}{4}}$  is a scaling variable that is most meaningfully defined in the inertial sublayer of the atmosphere (Monin and Obukhov, 1954). However, it is often used as a shorthand for turbulence elsewhere in the atmospheric surface layer, with higher values indicating more turbulent conditions. The Obukhov length,  $L$ , is calculated as

$$L = \frac{-\overline{T_s} u_*^3}{\kappa g \overline{w' T_s'}} \quad (6)$$

where  $\kappa = 0.4$  is the von Kármán constant,  $g$  is the acceleration due to gravity, and  $T_s$  is the sonic air temperature, which is a good approximation of the virtual potential temperature (Kaimal and Gaynor, 1991). The values of  $L$ ,  $u_*$  and the TKE are calculated from 20 Hz observations at  $z \approx 22 \text{ m} \approx h_c$  on Met 4 preferentially, because it lies at the downstream edge of the forest in the direction of the prevailing wind. On dates for which Met 4 observations were unavailable, the observations were taken from Met 1 (Met 4 and Met 1 account for 512 and 18 days, respectively, of the 530 total).

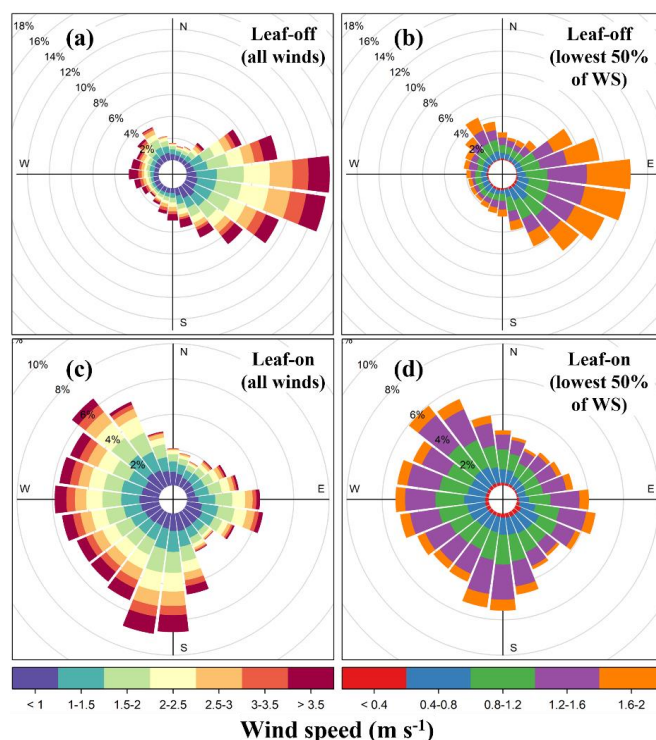
## 3 Results and Discussion

### 3.1 Wind conditions at BIFoR FACE

Figure 4 presents wind roses for the 2019–2021 fumigation period at BIFoR FACE across the period as a whole (Figure 4a, c) and for the observations used in the residence-time calculations, i.e., the lowest 50% of wind speeds across the whole



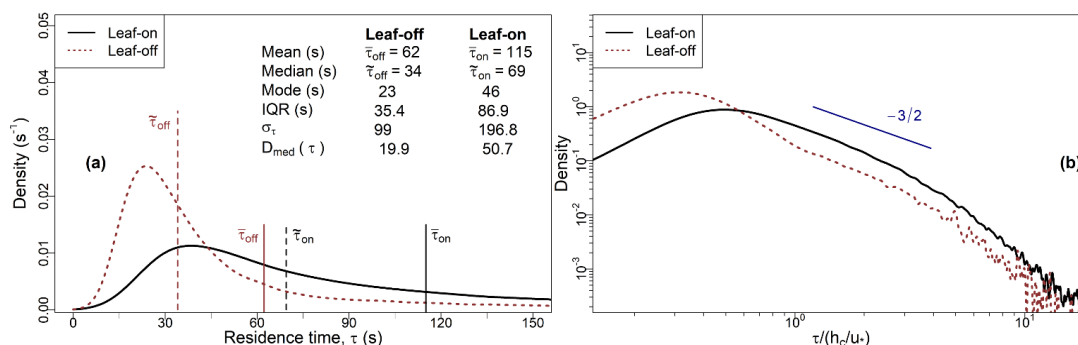
observation period (Figure 4b, d). The wind speeds are generally low compared with observations from most meteorological  
 305 stations because the wind measurements at BIFoR FACE are measured around the tops of the trees of each array, whereas  
 meteorological stations are typically located away from large obstacles. The wind speeds were generally higher in the leaf-off  
 period than the leaf-on. For example, 39% of 5-min averages were  $> 2.5 \text{ m s}^{-1}$  for the leaf-off period, compared with 27% for  
 leaf-on. The prevailing wind direction around BIFoR FACE is south-westerly, as is typical for most of the UK. However, the  
 wind direction in the UK is highly variable in April (leaf-off) and the wind direction around BIFoR FACE was predominantly  
 310 easterly during the leaf-off period 2019–2021 (Figure 4a, b). Predominantly easterly winds are unusual in the UK, but these  
 observations match the local synoptic conditions over the same period. Our leaf-off period is much shorter than the leaf-on  
 period and is therefore more susceptible to isolated meteorological events.



315 **Figure 4:** Wind roses for BIFoR FACE during the 2019–2021 leaf-off (a, b) and leaf-on periods (c, d). The wind roses are calculated  
 on 5-min averages of sonic measurements in array 1. (a, c) show wind roses across all wind conditions; (b, d) show wind roses for  
 the lowest 50% of wind speeds, used in the residence-time calculations. The wind roses for the other fumigation arrays are very  
 similar and are omitted to avoid repetition. Note the change of scale between (a, c) and (b, d).

### 3.2 Basic distributions of $\tau$ values

Figure 5 presents probability density functions (PDFs) and reports descriptive statistics of the residence times for the leaf-off  
 320 ( $\tau_{off}$ ) and the leaf-on ( $\tau_{on}$ ) periods. The overbar and overtilde notation refer to the mean and median values, respectively. The  
 modal values of  $\tau < \tilde{\tau} < \bar{\tau}$  for each period, which is typical but not diagnostic (von Hippel, 2005) of positively skewed unimodal  
 distributions. Longer residence times are relatively less common during the leaf-off period than leaf-on, as indicated by the  
 shift to the left of the  $\tau_{off}$  PDF compared with the  $\tau_{on}$  PDF. For example, 57% of  $\tau_{on}$  observations are greater than 60 s,  
 compared with only 24% of  $\tau_{off}$  values. The  $\tau_{on}$  values are more dispersed than the  $\tau_{off}$  values. For example, the interquartile  
 325 range (IQR) for  $\tau_{on}$  is over twice that of  $\tau_{off}$ , and  $D_{med}(\tau_{on}) > D_{med}(\tau_{off})$ , where  $D_{med}$  is the median absolute deviation.  
 In Figure 5b, both the leaf-off and leaf-on PDFs show clear modal values, followed by a region over which the decay exhibits  
 almost power-law behaviour, followed by steeper decay in the tails.



330 **Figure 5:** (a) PDFs and statistics of the residence times for the leaf-on and leaf-off periods. Solid and dashed vertical lines mark the mean and median values for each period, respectively. The mode for each period is taken as the value at which the PDFs attain their maximum densities. (b) As for (a), with PDFs presented on log-log axes with  $\tau$  normalised by  $h_c/u_*$ . The black line is the same as in Figure 3, although (a) presents dimensional information whereas Figure 3a presents the normalised PDF.

### 3.3 Dependence of $\tau$ on $u_*$ and atmospheric stability

#### 3.3.1 Dependence of $\tau$ on $u_*$

335 Figure 6 presents combined scatter and density plots showing the variation of  $\tau$  with  $u_*$  in the (a) leaf-off and (b) leaf-on periods. The warmer colours indicate regions of higher density. The colour scale is normalised to account for the different sample sizes in the two periods. Figure 6 shows, over both periods, the residence times decrease with increasing values of  $u_*$ . This accords with intuition that canopy residence times should progressively reduce with increasing turbulence. Most notably, (a) and (b) regress to gradients of  $\approx -1$  ( $-0.93$  and  $-0.95$ , respectively), which indicates that, as a first approximation, the effect of turbulence levels on the residence times is given by  $\tau \propto u_*^{-1}$ , as proposed by GCF17. It is worth qualifying this point a little. Because our  $u_*$  values are derived from a single measurement location whereas our  $\tau$  values in three nearby locations within 300 m (Figure 1), this argument assumes a state of “moving equilibrium” (Yaglom, 1979), in which  $u_*$  varies slowly in the  $x, y$  plane, with  $u_*$  measured at  $z = h_c$  serving as a local velocity scale. This assumption has not been tested in patchy forests such as that at BIFoR FACE, whose structure varies strongly in the  $x, y$  plane, likely challenging the assumption that  $u_*$  is approximately constant. Further, our results do not account for the effect of strong winds on  $\tau$ , which to our knowledge remains untested.

340

345

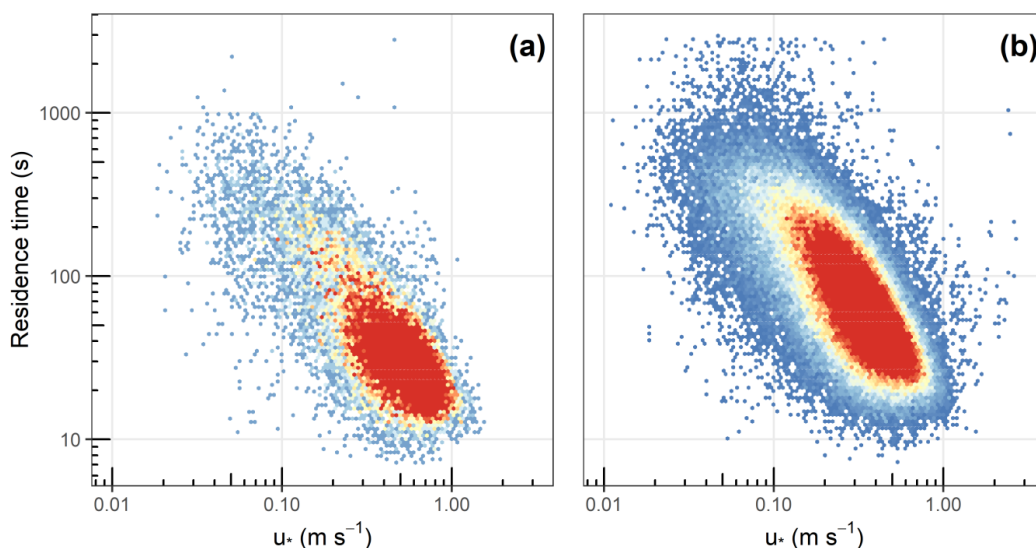


**Figure 6: Combined scatter and density plots, showing the variation of  $\tau$  with  $u_*$  for the leaf-off (a) and leaf-on (b) periods**

### 3.3.2 Dependence of $\tau$ on atmospheric stability

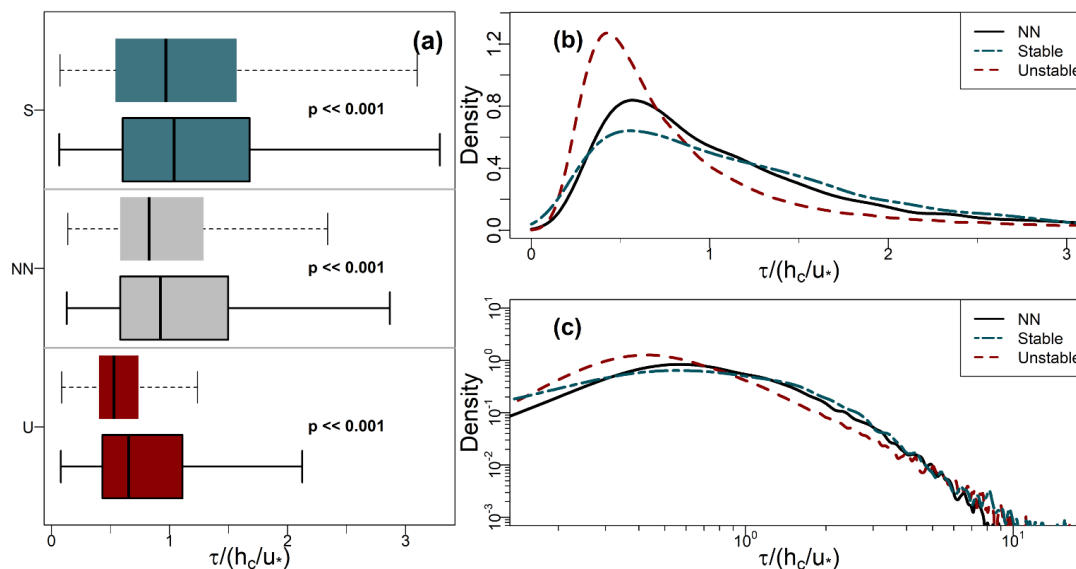
350 To analyse the dependence of  $\tau$  on atmospheric stability, we define three broad stability classes following the approach in Mahrt et al. (1998) and Dupont and Patton (2012). Our stability regimes are defined at  $z \approx h_c$  according to the behaviour of the kinematic fluxes of temperature  $\overline{w'T'_z}$  and momentum (via  $u_*$ ), as a function of the stability parameter  $h_c/L$  from Eq. (6).

- Near-neutral (NN):  $-0.005 \leq h_c/L < 0.003$ . In this regime, the momentum flux is significant, but the temperature flux is negligible.
- 355 • Stable:  $3 \leq h_c/L < 20$ . This regime occurs mostly in light winds, often on cloudy mornings or shortly before fumigation shutdown in the evening. The momentum flux is small. Intermittent turbulence is a major component of turbulent exchange (Mahrt, 2014).
- Unstable:  $-20 \leq h_c/L < -1$ . This regime mostly occurs during the day, especially in clear-sky conditions. This regime is characterized by a large temperature flux and, usually, small  $u_*$  values associated with light winds.

360

These thresholds are not universal and are site and study specific. We define only three broad stability classes and adopt unusually demanding thresholds to define them. This is because (i) fumigation is carried out mostly during the day, so we have limited opportunity to investigate transitory sub-regimes, which typically occur in the early morning and late evening; and (ii) the observations used to calculate  $L$  are not taken at exactly the same location as the observations used to calculate  $\tau$ , so we prefer to exclude potentially misleading marginal cases. Figure 7a shows box-whisker plots of  $\tau$  for the three stability regimes and Table 2 summarises their basic statistics. Figures 7b, c present PDFs for the three regimes during the leaf-on period (those for leaf off are similar and are included in Figure A1 in Appendix B). The values of  $\tau$  in Figure 7 are normalised by  $\tau_c = h_c/u_*$  for each class to minimise the more trivial dependence of  $\tau$  on  $u_*$ , because  $u_*$  varies between the classes. However, Table 2 presents the statistics in dimensional form for easier interpretation.

365



370

**Figure 7:** Statistics of normalised residence times binned by stability class (a) Box-whisker plots of normalised residence times for stable (S), near-neutral (NN), and unstable (U) conditions. Boxes with dashed whiskers and no border show leaf-off values; boxes with solid whiskers and borders show leaf-on. Solid vertical lines indicate median values. Width of the boxes shows the IQR. Lower and upper whiskers respectively indicate the 25<sup>th</sup> percentile  $-1.5 \times \text{IQR}$  and 75<sup>th</sup> percentile  $+1.5 \times \text{IQR}$ . (b) and (c) PDFs of residence times for the leaf-on period, plotted on linear and logarithmic axes (base 10), respectively.

375

**Table 2:** Descriptive statistics of  $\tau$  values for the leaf-on and leaf-off periods binned into three stability regimes. All values in seconds rather than normalised units. The symbols  $\bar{\tau}$ ,  $\sigma_{\tau}$ ,  $\tilde{\tau}$ , and  $D_{med}(\tau)$  denote the mean, standard deviation, median, and median absolute deviation, respectively.

	Stable		NN		Unstable	
	Leaf-on n = 11,291	Leaf-off n = 1,556	Leaf-on n = 10,668	Leaf-off n = 2,865	Leaf-on n = 32,001	Leaf-off n = 8,846
$\bar{\tau}$	229	155	100	64	89	37
$\sigma_{\tau}$	319	198	172	83	154	45
$\tilde{\tau}$	169	117	73	45	55	27
$D_{med}(\tau)$	121	85	47	24	34	12
<b>IQR</b>	174	124	72	38	57	17

380

Air-parcel residence times increase with increasing stability, as does the dispersion in their values. These differences are significant, both between the growing periods and between the stability classes in each period ( $p < 0.001$  using the Mann–Whitney–Wilcoxon test). In unstable conditions, long residence times are much less common than they are in the NN or stable regimes. For example, in Figures 7b, and 7c, the right tails of the unstable PDF are lighter than those for NN and the stable regime. The distributions of  $\tau$  remain positively skewed for each stability class (e.g., the right whiskers are longer than the left in Figure 7a). These general patterns are not sensitive to the exact thresholds of  $h_c/L$  used to bin the data. Changes in the turbulence structure around the forest likely account for the main differences in the distributions of  $\tau$  across the three stability classes. In NN conditions, shear generated eddies around the tops of the trees dominate turbulent exchange (Bannister et al., 2022; Brunet, 2020; Finnigan, 2000). However, as stability decreases from NN to free convection in the unstable regime, the dominant turbulent structures around the forest transition from shear-layer vortices to thermal plumes. These thermal plumes have typical length scales several times larger than shear-layer vortices (Patton et al., 2016), which could result in more vigorous mixing in unstable conditions than NN, resulting in the smaller  $\tau$  values seen for the former than the latter (Figure 7). Conversely, in stable conditions, in-canopy turbulence is much weaker and more intermittent than in neutral or unstable

385

390



conditions, reflected in (i) the larger average values of  $\tau$  for the stable regime than the NN or the unstable regimes; and (ii) a greater likelihood of long  $\tau$  values, when air remains within the canopy until it is vented by infrequent, intermittent turbulence, as reflected in the heavy tails of the stable PDFs. Section 3.7 discusses intermittent venting in stable atmospheric conditions in more detail. For the NN and unstable regimes,  $\tau \propto u_*^{-1}$ , but  $\tau \propto u_*^{-0.8}$  in stable conditions.

### 3.4 Dependence of $\tau$ on wind direction

Figure 8 presents polar plots showing percentiles in  $\tau$  values with wind direction. The values of  $\tau$  are not completely symmetrically distributed with regards to wind direction. This is unsurprising because the BIFoR FACE forest is a complex, mature woodland, within which the species composition, tree age, and stand structure varies. Array 1 provides the clearest example of the heterogeneity in that the residence times are noticeably lower when the wind direction is from the south and south-east (Figures 8a and 8d). This is because array 1 is located at the southern edge of the forest (Figure 1) and therefore vulnerable to edge effects from southerly winds. However, in most mature forests, structural heterogeneity means that point observations are never likely to be entirely neutral with respect to wind direction, even when edges are accounted for. For example, the closest edge to arrays 4 and 6 is to the north (Figure 1). But arrays 4 and 6 are relatively more exposed to south-westerly and southerly winds, respectively, because the trees abutting the arrays in those directions are slightly shorter than those to the north.

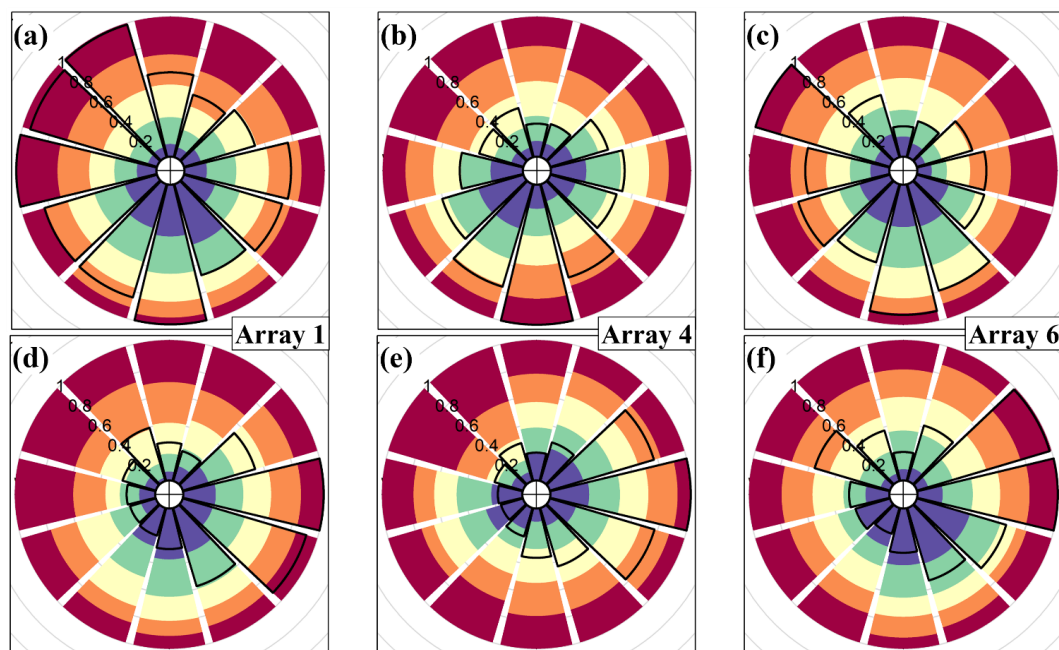


Figure 8: Residence-time quintiles by wind direction for the leaf-on (a–c) and leaf-off (d–f) periods. (a, d) Array 1; and (b, e) Array 4; and (c, f) Array 6. The colours indicate the proportion of  $\tau$  values within each quintile for each wind sector, increasing from purple (lowest 20% of  $\tau$  values) to red (highest 20% of  $\tau$  values). For example, (a) shows that for southerly winds, a higher proportion of  $\tau$  values are in the first and second quintiles than in the fifth (lower  $\tau$  values are more common). The solid black line shows the relative frequency of each wind sector, with the scale 0–1 indicated by the radial numbering

No systematic differences or symmetries are apparent between the southern-edge array (array 1) and the northern-edge arrays (4 and 6). Because wind directional effects are so site and climate specific, it is difficult to generalise these results other than to say, where possible, observational campaigns of forest-atmosphere exchange in patchy landscapes should include at least two measurement locations, one deep in the forest, and one near any edges, especially in the direction of the prevailing wind. Forest edges experience different wind conditions, chemistry, microclimates to forest interiors (Bonn et al., 2014; Schmidt et



al., 2017). It is important not to dismiss forest-edge processes as unrepresentative, however, because edges comprise the  
420 majority of the forested area in many parts of the world (Bannister et al., 2022).

### 3.5 Seasonal (leaf-on/leaf-off) differences in $\tau$

As indicated by the descriptive statistics in section 3.2, the forest is more ventilated when the trees are not in leaf. Taking the  
distributions of  $\tau$  across the entire fumigation period, the values of  $\tau_{on}$  are significantly higher than the values of  $\tau_{off}$ , with  
 $p \ll 0.001$  using both the  $t$ -test and the Mann–Whitney–Wilcoxon test. Figure 8 shows that, for a given percentile,  $\tau_{on} < \tau_{off}$   
425 for most wind directions, particularly in arrays 1 and 4, which are slightly less sheltered than array 6. Figure 7 and Table 2  
shows the average values of  $\tau_{off} < \tau_{on}$  for the three stability classes we defined, with the distributions remaining significantly  
different ( $p \ll 0.001$ ). The dispersion in the  $\tau_{on}$  values is higher than in  $\tau_{off}$  across the entire fumigation period, and in  
unstable conditions. However, for the NN and stable regimes, the dispersion in the  $\tau$  values is quite similar between the two  
periods.

### 430 3.6 Comparison with published residence time values

Recalling the set-up of the FACE operations, described above, our estimates are most comparable to the daytime residence  
times of air parcels released from approximately the upper two-thirds of the canopy,  $z/h_c > 1/3$ . With these considerations  
in mind, our calculated residence times fall within the range of modelled median values of tens of seconds to a few minutes  
(Fuentes et al., 2007; Gerken et al., 2017; Strong et al., 2004). There are few reported observational estimates of residence  
435 times, and none derived from measurements in ecosystems similar to the BIFoR FACE forest. To the extent a comparison is  
meaningful, our calculated residence times are within the range of reported field estimates e.g., mean values of a minute or  
two during the growing season (Farmer and Cohen, 2008; Martens et al., 2004).

Our results agree with existing modelling studies that the distributions of residence times are strongly positively skewed and  
440 in certain conditions—e.g., in stable conditions (Figure 7) or for parcels travelling from near the ground (GCF17; Strong et  
al., 2004)—can be widely dispersed with quite heavy tails. For these situations, average values cannot be said to be  
'representative', and it is preferable to be able to estimate distributions rather than single values. GCF17's model in Eq. (1) is  
appealing because it allows the distribution to be estimated from a small set of variables, making it suitable for deployment in  
large-scale models. The eddy diffusivity  $K_{eq}$  can be partially tuned to account for the forest structure and wind conditions.  
445 However, although GCF17's model generates modal values similar to those we observed, it appears to overpredict the  
likelihood of long residence times in the upper canopy. For example, GCF17 predicts around 20% of air parcels have residence  
times of five minutes or more whereas, in our leaf-on data, the proportion is closer to 6%. Some of the discrepancy between  
our observations and GCF17's model likely results from our underestimation of  $\tau$  because of the finite-size arrays used in the  
mass balance calculations in Eq. (5). However, given that GCF17's model and our results diverge even in low winds, when  
450 advection is negligible and turbulence is weak, this factor is unlikely to be the only relevant difference. Indeed, the tails of  
GCF17's own LES-generated PDFs appear to decay faster than the  $-3/2$  power law predicted by analytical model in Eq. (1)—  
especially for parcels released higher in the canopy—further suggesting Eq. (1) overpredicts the likelihood of long residence  
times.

455 The eddy-diffusivity closure assumptions used to formulate Eq. (1) are most realistic when the length and time scales of the  
transport mechanism are smaller than the scale of the gradients in the measured quantities (Corrsin, 1975). Cava et al. (2006)  
show this condition is most likely to be satisfied when the sum of the turbulent transport and buoyant production terms in the  
transport equations is small compared to the gradient in the measured quantity. In forests and other vegetation canopies in



neutral conditions, this is a reasonable assumption below around  $z/h_c = 1/2$ , especially when considering quantities with  
460 strong gradients, such as fertilizer (Bash et al., 2010) or fungal spores. However, in forest crowns in neutral conditions,  
turbulent exchange is dominated by eddies with diameters that scale with  $h_c$  (Brunet, 2020; Finnigan, 2000; Raupach et al.,  
1996). These eddies create significant turbulent transport, meaning that the eddy-diffusivity model underestimates turbulent  
forest-atmosphere exchange in the upper canopy and therefore overestimates residence times. As a more general consideration,  
GCF17's model envisages a horizontally homogeneous, quasi-infinite forest, in which the only path of exit for air parcels is  
465 via turbulent exchange at the top of the canopy. However, real forests usually comprise a patchwork of gaps and clearings at  
all heights, caused by disease, tree senescence, human activities, and wind throw. These openings offer air parcels additional  
routes to exit forests, such as via advection across edges or through the regions of strong turbulent fluxes that form in patchy  
forest crowns. In hilly terrain, flow-separation regions in the lee of hills can create chimney-like pathways for air parcels to  
leave the forest, particularly for parcels moving from near the ground (Bannister et al., 2022; Chen et al., 2019). The likely net  
470 effect of these additional pathways is to reduce the incidence of very long residence times, particularly in forests with extensive  
edge regions and patchy structures.

Here we adapt GCF17's model to reduce the overprediction of large  $\tau$  values while keeping it simple enough to be deployed  
in regional or global models, for which information on the canopy structure and the flow of air is typically limited. First, we  
475 observe that Eq. (1) is a special case of the inverse-gamma distribution, the general form of which is

$$p(\tau; \alpha, \beta) = \frac{\beta^\alpha}{\Gamma(\alpha)} \tau^{-(\alpha+1)} \exp[-\beta/\tau]; \tau > 0, \quad (7)$$

where  $\Gamma(\cdot)$  is the gamma function and  $\alpha$  and  $\beta$  are, respectively, shape and scale parameters ( $\beta$  is the rate parameter from the  
point of view of the gamma distribution). Taking  $\alpha = 1/2$  and  $\beta = \tau_{\text{turb}} = (h_c - z_{\text{rel}})^2 / 4K_{eq}$  in Eq. (7) gives Eq. (1). The  
value of  $\beta$  is relatively more influential at lower values of  $\tau$ , whereas  $\alpha$  determines the distribution's dominant behaviour for  
large  $\tau$ . In forest crowns, turbulent exchange scales with the canopy turnover timescale  $\tau_c = h_c/u_*$ , which we use as our value  
480 for  $\beta$ . The value of  $\alpha$  then determines the shape of the distribution, particularly at large  $\tau$  values. We find  $\alpha = 1.4-1.8$  fits our  
observations better than using  $\alpha = 1/2$ , as in GCF17 (Figure 9). The main effect of the larger  $\alpha$  value is to reduce the probability  
of very long residence times, as evidenced by the roll-off of our PDFs from GCF17 at large  $\tau$  values in Figure 9. A helpful by-  
product is that, for  $\alpha > 1$  in Eq. (7), the mean values of  $\tau$  become formally defined as  $\bar{\tau} = \beta/(\alpha - 1)$  (the mean is undefined  
for  $\alpha < 1$ ). For our data,  $\tau_{c(\text{on})} = 78$  s and  $\tau_{c(\text{off})} = 54$  s. Taking  $\alpha = 1.6$  and  $1.8$  as rough estimates for the leaf-on and leaf-  
485 off periods, respectively, gives  $\bar{\tau}_{\text{on}} = 130$  s and  $\bar{\tau}_{\text{off}} = 68$  s, close to the values  $\bar{\tau}_{\text{on}} = 115$  s and  $\bar{\tau}_{\text{off}} = 62$  s calculated directly  
on our data.

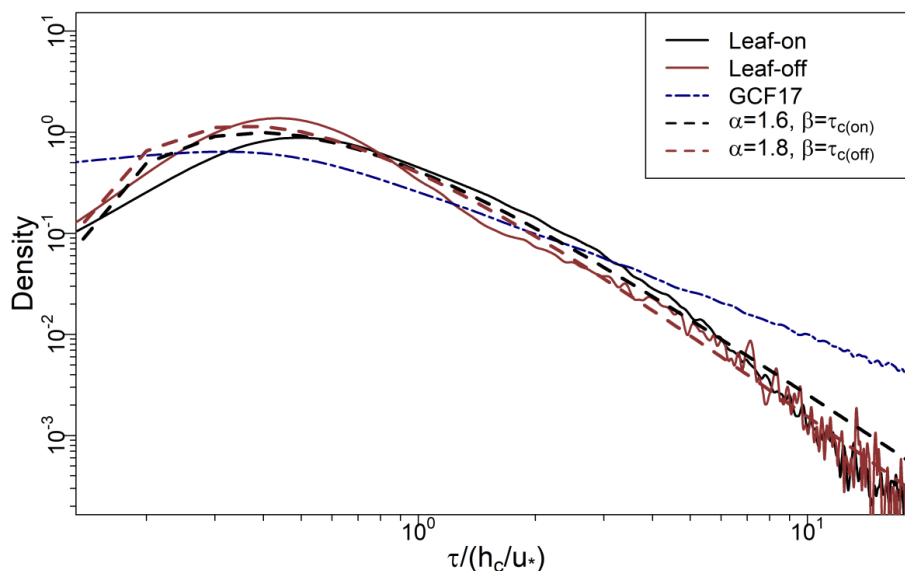


**Figure 9:** Solid black and red lines show PDFs of  $\tau$  from BIFoR FACE during the leaf-on and leaf-off periods, respectively. Dashed lines show PDF estimates on the BIFoR FACE observations using Eq. (7). Dot-dash navy line shows PDF from GCF17 in Eq. (1).  $\tau_{c(on)}$  and  $\tau_{c(off)}$  denote  $\tau_c = h_c/u_*$  for the leaf-on and leaf-off periods. All  $\tau$  values normalised by  $\tau_c = h_c/u_*$ .

Inverse-gamma distributions are flexible and can fit observations from a variety of processes, without always reflecting the underlying physical mechanisms. However, surface renewal theory (SRT) (Danckwerts, 1951) offers a compelling analogy that warrants further testing with physical models or LES. SRT assumes the movement of individual fluid parcels near a surface may be represented as a stochastic process driven by a turbulent flow field away from the surface, which is comparable, at least conceptually, to air parcels moving to and from a porous forest canopy exposed to the open atmosphere. SRT has been used to estimate the fluxes of scalar quantities to and from forests (Katul et al., 2013; Paw U et al., 1995). Under certain SRT assumptions, it has been shown that residence times can be well approximated using distributions in the gamma family (Gon Seo and Kook Lee, 1988; Haghighi and Or, 2013, 2015; Katul and Liu, 2017; Zorzetto et al., 2021). We hope a similar approach may be used to estimate  $\alpha$  for other forest types, for example, by using LES to calculate  $\tau$  across a variety of realistic forests (i.e., including openings, edges, and horizontally heterogeneous structure).

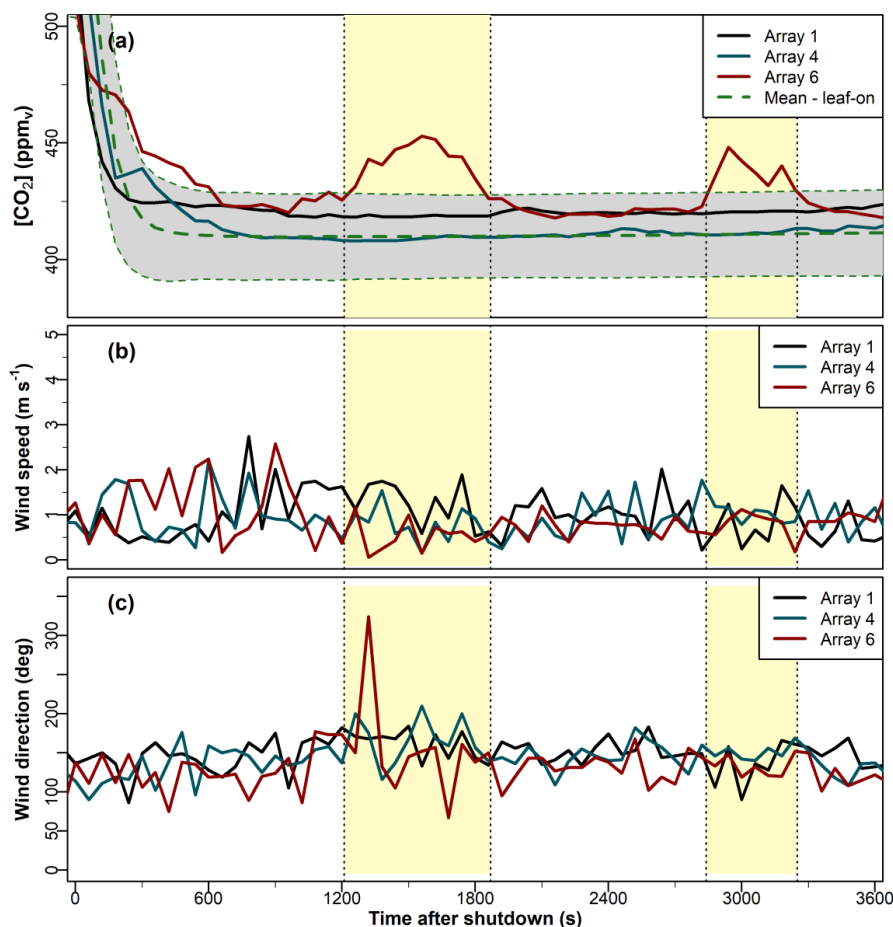
We reiterate here that the above discussion does not include the effect of very strong winds on  $\tau$  (see section 2.3), which also lends itself to further testing with LES. We expect  $\alpha$  to increase slightly in strong winds, when the reconfiguration of tree crowns allows energetic gusts to penetrate further and more regularly into the forest canopy. The behaviour of  $\tau$  across atmospheric stability regimes is more difficult to parametrise. We obtain good fits on both our leaf-on and leaf-off observations in unstable conditions using  $\beta = 2h_c/w_*$  in Eq. (7), where  $w_* = (g\overline{w'T_s'}h_c/\overline{T_s})^{1/3}$ , the Deardorff convective velocity scale (defined locally). However, we do not have sufficient spatial resolution in our observations to determine whether this result is robust across a range of unstable conditions, or whether it is just a consequence of the flexibility of the inverse-gamma distribution. In stable conditions, turbulence is dominated by turbulent structures that are intermittent in space and time. These intermittent structures can induce complex flow patterns that do not lend themselves to scaling analysis. The following subsection discusses evidence of this complex behaviour and its implications for air-parcel residence times.

### 3.7 Longer residence times evidenced by evening venting events

On some evenings during the leaf-on period, we observed ‘bumps’ in the  $[\text{CO}_2]$  time series shortly after fumigation was shut down, whereby the  $[\text{CO}_2]$  decays to  $a[\text{CO}_2]$ , rises again by tens of  $\mu\text{mol mol}^{-1}$  for several minutes, before decaying again to



515 a[CO<sub>2</sub>]. Figure 10 shows a representative example from 17 August 2020. Pools of CO<sub>2</sub> can accumulate naturally in forests, e.g., from soil respiration on calm, humid nights, creating anomalously high carbon flux values when the pools are vented from the canopy (Cook et al., 2004). The venting of natural pools typically occurs in the early hours of the morning, after the CO<sub>2</sub> has had time to accumulate in the stable nocturnal conditions (Cook et al., 2004), and can last for several hours. Here, the bumps occur shortly after shutdown, last for no more than a few minutes, and occur only in the fumigation arrays. We therefore  
520 believe these bump signals are evidence of the venting from the canopy of trapped fumigation CO<sub>2</sub> within the canopy, rather than of natural pools (although without isotope analysis it is not possible to conclude with absolute certainty). To investigate these bumps further, we filtered the data according to the following criteria: at least 15 minutes after the shutdown time, the [CO<sub>2</sub>] in one or more of the arrays rises by  $\geq 15 \mu\text{mol mol}^{-1}$  from the a[CO<sub>2</sub>] for  $\geq 3$  minutes. These criteria are somewhat arbitrary but serve to distinguish the signal from the inevitable noise as the [CO<sub>2</sub>] decays to a[CO<sub>2</sub>]. These criteria identified  
525 41 days with bump events during the leaf-on period, from a total of 452 observation days (i.e., about 9% of the time). Using these criteria, no bumps occurred in the leaf-off period.

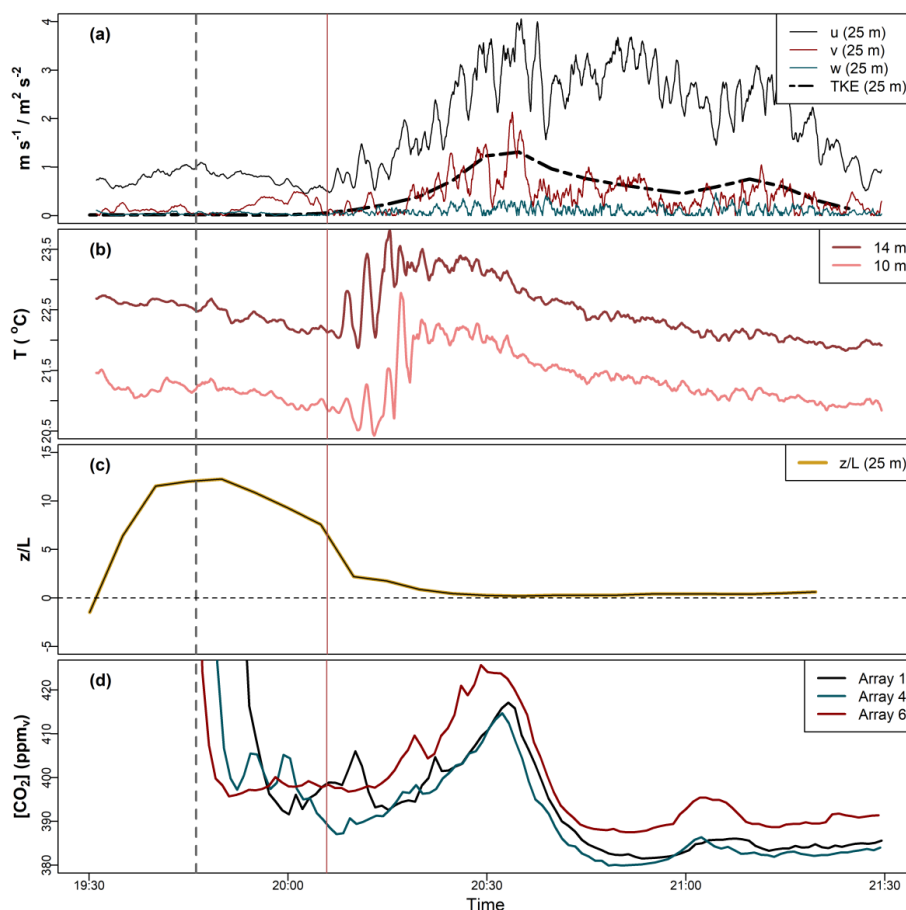


530 **Figure 10: Time series of 1-minute averages in (a) the [CO<sub>2</sub>], (b) wind speed, and (c) wind direction after shutdown on 17 Aug 2020. In panel (a), the dashed green line shows the mean [CO<sub>2</sub>] at each 1-minute time step after shutdown for the leaf-on period. The grey shaded confidence interval in (a) shows one standard deviation either side of the mean. The shaded yellow rectangles indicate the approximate duration of the venting events.**

The bumps occurred only when wind speeds were low, all with  $\bar{u} < 1.5 \text{ m s}^{-1}$  and typically with  $\bar{u} < 1 \text{ m s}^{-1}$ . This was a necessary but not sufficient condition; there were days with weak winds but no bump events in the [CO<sub>2</sub>] time series. These bump events may be caused by CO<sub>2</sub>-rich air being trapped within the dense canopy, particularly when the surrounding



535 atmospheric conditions are very stable, which can occur on evenings with low winds and strong stratification from radiative  
cooling. The venting occurs when intermittent turbulent structures interact with the forest airspace (whose local stability may  
differ to that of the surrounding atmosphere). In very stable conditions, boundary-layer turbulence is intermittent in space and  
time, and may arise from with a variety of phenomena, such as differential heating, top-down turbulent bursts, or larger  
'submeso' motions such as microfronts and short gravity waves (Mahrt, 2014; Wharton et al., 2017). These turbulent structures  
540 tend to be highly localised, which could explain why the bumps in our time series rarely occurred in more than one array at  
any one time, even though they typically last for 10 minutes or so (Figure 10). Detecting intermittent turbulent structures  
around forests requires dense networks of 3D anemometers throughout the canopy, which BIFoR FACE did not have for most  
of our investigation period (we have recently installed several anemometers within the forest for future investigations).  
However, on a few occasions, the meteorological towers around the edge of the forest were able to detect the presence of  
545 submeso structures.



550 **Figure 11:** Time series after shutdown on 27 Aug 2019 of (a) the magnitude of the velocity vector components ( $\text{m s}^{-1}$ ) and TKE ( $\text{m}^2 \text{ s}^{-2}$ ) at  $z = 25 \text{ m}$ , (b)  $T$  ( $^{\circ}\text{C}$ ), (c)  $z/L$  (where  $L$  is the Obukhov length), and (d)  $[\text{CO}_2]$ . The dashed grey vertical line indicates the shutdown time and the solid red line the approximate arrival time of the warm microfront. The high-resolution measurements in (a)–(c) are from on Met1, at the southern edge of the BIFoR FACE facility (Figure 1). (a) and (b) show 1-min rolling means.

Figure 11 presents a case study from 27 August 2019, which was a warm, cloudless day with weak southerly winds. Around sunset, and therefore fumigation shutdown (marked with the dashed grey vertical line in Figure 11), the wind speed was very low—less than  $1 \text{ m s}^{-1}$  at  $z = 25 \text{ m}$  at the forest edge (Figure 11a) and almost zero within the canopy. The TKE was close to zero (Figure 11a). A strong temperature inversion formed (Figure 11b), with the temperature at  $z = 25 \text{ m}$  a further few degrees



555 warmer than at  $z = 14$  m (not shown). The air around the forest was very stable, with  $z/L \approx 10$ –15 (Figure 11c). Around 20  
minutes after shutdown, a warm microfront reached the southern edge of the forest, marked with the solid vertical red line in  
Figure 11 and visible in a sharp increase in temperature near the ground (Figure 11b). The passage of warm microfront leads  
to increased local wind speed and turbulent intensity, and decreased atmospheric stratification (Mahrt, 2019). These changes  
can be seen in Figure 11a, where the horizontal wind speed and the TKE increase quickly, and Figure 11c, which shows the  
560 stability decaying quickly from very stable to approximately neutral (i.e.,  $z/L \approx 0$ ). The increased wind speed and turbulence  
cause trapped  $\text{CO}_2$  to be vented from the forest in all the fumigation arrays (Figure 11d). As well as providing interesting  
micrometeorological case studies, these venting events provide observational evidence that air-parcel residence times can be  
much longer in stable evening conditions compared with the average daytime values, e.g., at least 20–30 minutes in the example  
in Figure 11 and nearly 60 minutes in the example in Figure 10.

#### 565 4 Conclusions

Our opportunistic investigations of fumigation data from the BIFoR FACE facility provide the first observational evidence of  
air-parcel residence times in the upper canopy of a deciduous forest. Air-parcel residence times in the upper half of the forest  
canopy vary strongly with atmospheric stability, and their statistics differ significantly when the forest is in leaf compared to  
when it is not. Our dataset shows that air parcels in the BIFoR FACE facility have the following characteristics:

- 570 1. When the trees are in leaf, we found median daytime residence times,  $\bar{\tau}$ , are around twice as long ( $\bar{\tau} \approx 70$  s) as when  
the trees are not in leaf ( $\bar{\tau} \approx 34$  s). The dispersion in the values of  $\tau$  is over twice as large when the trees are in leaf  
versus when they are not in leaf, e.g., median absolute deviation,  $D_{med} \approx 51$  s for leaf-on and  $D_{med} \approx 20$  s for leaf-  
off.
- 575 2. For chemically reactive tracers, such as BVOCs, released in the upper canopy during daytime, our results suggest the  
molecules are unlikely to have time to react within the forest unless their reaction time scale is in the order of a few  
minutes or less.
- 580 3. Our results agree with Lagrangian modelling studies that the distributions of  $\tau$  are strongly positively skewed (e.g.,  
Figure 4). For these types of distributions, average values are not representative of the population as a whole. Where  
possible, future investigations should report the distributions of residence times, or at least a dispersion measure to  
accompany average values. Median values, accompanied by the interquartile range or  $D_{med}$ , are preferable to the  
mean and standard deviation because the former are more robust measures of highly positively skewed distributions.
- 585 4. The PDFs of residence times can be closely approximated using the inverse-gamma distribution. Models using eddy-  
diffusivity turbulence closure generate plausible average values but overestimate the probability of very long  
residence times in the upper canopy (i.e., the PDF tails are too heavy). We find the canopy turnover timescale,  $\tau_c =$   
 $h_c/u_*$ , provides a good approximation for the scale parameter of the inverse-gamma distribution, with the shape  
parameter a function of the forest's structure. Although outside the scope of the present study, we suggest that careful  
testing using physical models or LES will be able to generate robust residence time parametrisations based on simple  
gamma-like distributions, where the shape and rate/scale parameters can be estimated from variables such as the LAI  
or wind-velocity statistics, which are available at most forest research sites and, increasingly, at all forest locations  
590 from remote sensing.
5. Air-parcel residence times increase with increasing stability, as does the dispersion in their values. In unstable  
conditions, long residence times are much less common than they are in near-neutral or stable conditions. In neutral  
and unstable conditions, the effect of turbulence levels on the residence times can be approximated  $\tau \propto u_*^{-\gamma}$ . Our  
data show  $\gamma \approx 1$  in unstable and neutral conditions, but  $\gamma \approx 0.8$  in stable conditions.



- 595 6. Very long residence times (tens of minutes to hours) can occur in the evening boundary-layer transition when the  
trees are in leaf. These are evidenced in our data by the venting of trapped CO<sub>2</sub> from the canopy long after FACE  
fumigation has been shut down for the day. This behaviour occurs on a little fewer than 10% of the days with suitable  
meteorology in our dataset. Cook et al. (2004) report nocturnal venting of pooled CO<sub>2</sub> over the course of several  
hours, which is different from what we see here. We are not aware of any other observational evidence of these brief  
600 evening venting events, which typically last around 5–20 minutes and are highly localised, usually in a single  
fumigation patch. The evening venting events occur only in low winds. We suspect they are evidence of the decoupled  
forest air space interacting with intermittent turbulent structures in very stable conditions. We found a single case  
study of a warm microfront, a type of ‘submeso’ atmospheric motion, causing venting of the forest air space, but the  
causes of the majority of venting events are not known.
- 605 7. The observation of these venting events, and the long residence times they imply, fits with previous field studies that  
nocturnal residence times are often in the order of several hours, rather than the few minutes typical of daytime values  
(Martens et al., 2004; Rummel et al., 2002). The stable boundary layer, particularly during the evening and at night,  
remains poorly understood. Further investigations of nocturnal residence times are needed to understand how physical  
processes determine in-canopy chemistry, e.g., the mixing ratios of monoterpenes in boreal forests are at their highest  
610 at night, but those for isoprene are at their lowest (Hakola et al., 2012). These investigations need to be centred around  
robust observations and physical experiments—nocturnal exchange is dominated by intermittent turbulence that is  
difficult to constrain in numerical models (Bannister et al., 2022; Mahrt, 2014; Sterk et al., 2016).

*Data availability.* The time-averaged measurements, supporting README files, and visualisation code for this work are  
615 deposited in the following open-access repository: <https://doi.org/10.25500/edata.bham.00000836>. The raw BIFoR FACE  
measurements are publicly accessible at <https://doi.org/10.25500/edata.bham.00000564> – see Hart et al. (2020) and  
MacKenzie et al. (2021) for further detail.

*Author contributions.* EJB conceived of the study, wrote the processing code, conducted the formal analysis and visualisation,  
and wrote the original draft, under the supervision of ARMK, MJ, and XMC, who provided regular feedback on the  
620 methodology and original draft. KMH, MJH, GC are responsible for the operation of the BIFoR FACE facility and the curation  
of the data arising from it. All authors contributed to reviewing and editing the manuscript.

*Competing interests.* The authors declare that they have no conflict of interest.

*Acknowledgments.* The BIFoR FACE facility is a research infrastructure project supported by the JABBS Foundation and the  
University of Birmingham. The authors gratefully acknowledge additional funding from the John Horseman Trust, the  
625 Ecological Continuity Trust and the UK Natural Environment Research Council (NERC, grant NE/S015833/1) in support of  
this work and the wider research at the BIFoR FACE facility. It is EJB’s pleasure to acknowledge the Natural Environment  
Research Council (NERC) for funding through a CENTA studentship (grant NE/L002493/1). Photograph of the infrastructure  
in Figure 1 (bottom right of figure) taken by Andrew Priest Photography. The authors thank Chantal Jackson for her help in  
drawing and compiling Figure 1. We conducted the data analysis and statistical calculations using R (R Core Team, 2021),  
630 including the openair package (Carslaw and Ropkins, 2012), and Python.

#### Appendix A – Estimating $K_{eq}$ in Eq. (1)

A variety of methods can be used to estimate  $K_{eq}$  around vegetation (Haverd et al., 2009; Monteith and Unsworth, 2008). We  
use GCF17’s simple parametrization



$$K_{eq} = T_l g(LAI) u_* h_c, \quad (A1)$$

635 where  $h_c$  is the mean height of the canopy,  $u_*$  is the friction velocity measured at a height  $h_c$ ,  $T_l$  is the Lagrangian integral time scale normalised by  $h_c/u_*$ , and  $g(LAI)$  is a function that adapts the profile of the vertical velocity variance to the canopy structure such that

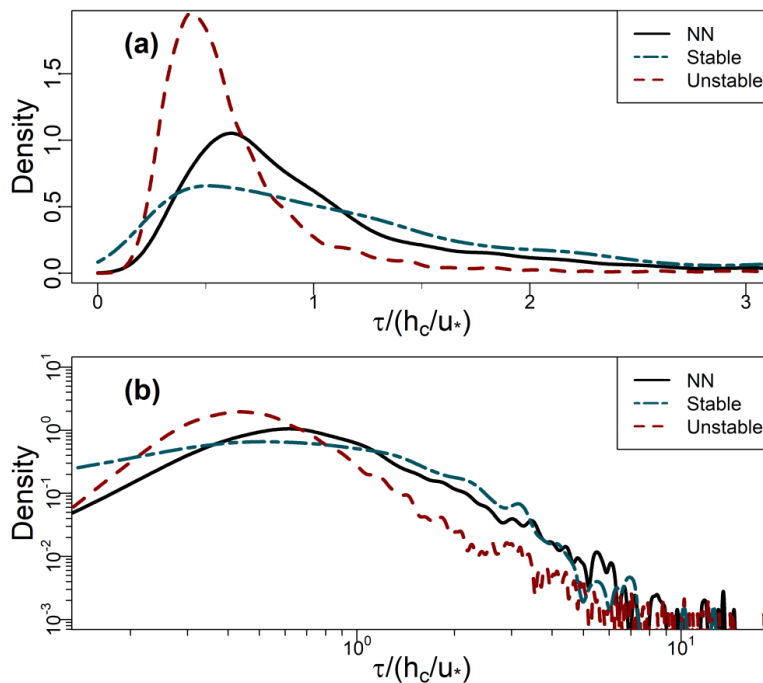
$$g(LAI) = c_1^2 \frac{2c_2 - 4 \exp(c_2) + \exp(2c_2) + 3}{2c_2 (\exp(c_2) - 1)^2} \quad (A2)$$

where  $c_1$  and  $c_2$  are modelling constants, with  $c_1 = 0.9$  and  $c_2 \approx -0.5-1.5$ . GCF17 use  $T_l = 1/3$  from Raupach (1989), but we  
 640 obtain better results on our data using the estimate of Haverd et al. (2009) such that

$$T_l = c_4 \frac{1 - \exp(-c_3 z_{rel}/h_c)}{1 - \exp(-c_3)}, \quad (A3)$$

where  $c_3 = 4.86 \pm 1.52$  and  $c_4 = 0.66 \pm 0.1$ , which gives  $T_l \approx 0.6$ . Taken together, these assumptions obtained  $K_{eq} = 1.2 \text{ m}^2 \text{ s}^{-1}$ , which was used in Eq. (1) to generate the GCF17 PDF in Figure 3, for example.

## Appendix B



645



**Figure A1: (a) and (b) PDFs of residence times binned by stability class for the leaf-off period, plotted on linear and logarithmic axes (base 10), respectively. NN denotes near-neutral conditions. See section 3.3.2 for definitions and Figure 7b, c for analogous results from the leaf-on period**

## References

- 650 Von Arnold, K., Nilsson, M., Hånell, B., Weslien, P. and Klemedtsson, L.: Fluxes of CO<sub>2</sub>, CH<sub>4</sub> and N<sub>2</sub>O from drained organic soils in deciduous forests, *Soil Biol. Biochem.*, 37(6), 1059–1071, doi:10.1016/j.soilbio.2004.11.004, 2005.
- Aubinet, M., Feigenwinter, C., Heinesch, B., Bernhofer, C., Canepa, E., Lindroth, A., Montagnani, L., Rebmann, C., Sedláč, P. and Van Gorsel, E.: Direct advection measurements do not help to solve the night-time CO<sub>2</sub> closure problem: Evidence from three different forests, *Agric. For. Meteorol.*, 150(5), 655–664, doi:10.1016/j.agrformet.2010.01.016, 2010.
- 655 Bailey, B. N., Stoll, R., Pardyjak, E. R. and Mahaffee, W. F.: Effect of vegetative canopy architecture on vertical transport of massless particles, *Atmos. Environ.*, 95, 480–489, doi:10.1016/j.atmosenv.2014.06.058, 2014.
- Bannister, E. J., MacKenzie, A. R. and Cai, X. -M.: Realistic forests and the modeling of forest-atmosphere exchange, *Rev. Geophys.*, 60(1), 1–47, doi:10.1029/2021rg000746, 2022.
- Bash, J. O., Walker, J. T., Katul, G. G., Iones, M. R., Nemitz, E. and Robarge, W. P.: Estimation of in-canopy ammonia sources and sinks in a fertilized zea mays field, *Environ. Sci. Technol.*, 44(5), 1683–1689, doi:10.1021/es9037269, 2010.
- Bonn, B., Bourtsoukidis, E., Sun, T. S., Bingemer, H., Rondo, L., Javed, U., Li, J., Axinte, R., Li, X., Brauers, T., Sonderfeld, H., Koppmann, R., Sogachev, A., Jacobi, S. and Spracklen, D. V.: The link between atmospheric radicals and newly formed particles at a spruce forest site in Germany, *Atmos. Chem. Phys.*, 14(19), 10823–10843, doi:10.5194/acp-14-10823-2014, 2014.
- 665 Brunet, Y.: Turbulent Flow in Plant Canopies: Historical Perspective and Overview, *Boundary-Layer Meteorol.*, 177(2–3), 315–364, doi:10.1007/s10546-020-00560-7, 2020.
- Cai, X.: Effects of differential wall heating in street canyons on dispersion and ventilation characteristics of a passive scalar, *Atmos. Environ.*, 51, 268–277, doi:10.1016/j.atmosenv.2012.01.010, 2012.
- Carslaw, D. C. and Ropkins, K.: Openair - An r package for air quality data analysis, *Environ. Model. Softw.*, 27–28, 52–61, doi:10.1016/j.envsoft.2011.09.008, 2012.
- 670 Cava, D., Katul, G. G., Scrimieri, A., Poggi, D., Cescatti, A. and Giostra, U.: Buoyancy and the sensible heat flux budget within dense canopies, *Boundary-Layer Meteorol.*, 118(1), 217–240, doi:10.1007/s10546-005-4736-1, 2006.
- Chen, B., Chamecki, M. and Katul, G. G.: Effects of topography on in-canopy transport of gases emitted within dense forests, *Q. J. R. Meteorol. Soc.*, 145(722), 2101–2114, doi:10.1002/qj.3546, 2019.
- 675 Cook, B. D., Davis, K. J., Wang, W., Desai, A. R., Berger, B. W., Teclaw, R. M., Martin, J. G., Bolstad, P. V., Bakwin, P. S., Yi, C. and Heilman, W.: Carbon exchange and venting anomalies in an upland deciduous forest in northern Wisconsin, USA, *Agric. For. Meteorol.*, 126(3–4), 271–295, doi:10.1016/j.agrformet.2004.06.008, 2004.
- Corrsin, S.: Limitations of gradient transport models in random walks and in turbulence, *Adv. Geophys.*, 18(Part A), 25–60, doi:10.1016/S0065-2687(08)60451-3, 1975.
- 680 Danckwerts, P. V.: Significance of Liquid-Film Coefficients in Gas Absorption, *Ind. Eng. Chem.*, 43(6), 1460–1467, doi:10.1021/ie50498a055, 1951.
- Drake, J. E., Macdonald, C. A., Tjoelker, M. G., Crous, K. Y., Gimeno, T. E., Singh, B. K., Reich, P. B., Anderson, I. C. and



- Ellsworth, D. S.: Short-term carbon cycling responses of a mature eucalypt woodland to gradual stepwise enrichment of atmospheric CO<sub>2</sub> concentration, *Glob. Chang. Biol.*, 22(1), 380–390, doi:10.1111/gcb.13109, 2016.
- 685 Dupont, S. and Patton, E. G.: Influence of stability and seasonal canopy changes on micrometeorology within and above an orchard canopy: The CHATS experiment, *Agric. For. Meteorol.*, 157, 11–29, doi:10.1016/j.agrformet.2012.01.011, 2012.
- Edburg, S. L., Stock, D., Lamb, B. K. and Patton, E. G.: The Effect of the Vertical Source Distribution on Scalar Statistics within and above a Forest Canopy, *Boundary-Layer Meteorol.*, 142(3), 365–382, doi:10.1007/s10546-011-9686-1, 2012.
- Farmer, D. K. and Cohen, R. C.: Observations of HNO<sub>3</sub>, ΣN, ΣPN and NO<sub>2</sub> fluxes: Evidence for rapid HO<sub>x</sub> chemistry within a pine forest canopy, *Atmos. Chem. Phys.*, 8(14), 3899–3917, doi:10.5194/acp-8-3899-2008, 2008.
- 690 Finnigan, J. J.: Turbulence in Plant Canopies, *Annu. Rev. Fluid Mech.*, 32, 519–571, 2000.
- Forkel, R., Guenther, A. B., Ashworth, K., Bedos, C., Delon, C., Lathiere, J., Noe, S., Potier, E., Rinne, J., Tchepel, O. and Zhang, L.: Review and Integration of Biosphere-Atmosphere Modelling of Reactive Trace Gases and Volatile Aerosols, *Rev. Integr. Biosph. Model. React. Trace Gases Volatile Aerosols*, 169–179, doi:10.1007/978-94-017-7285-3, 2015.
- 695 Fuentes, J. D., Lerdau, M. T., Atkinson, R., Baldocchi, D. D., Bottenheim, J. W., Ciccioli, P., Lamb, B. K., Geron, C. D., Gu, L., Guenther, A. B., Sharkey, T. D. and Stockwell, W. R.: Biogenic Hydrocarbons in the Atmospheric Boundary Layer: A Review, *Bull. Am. Meteorol. Soc.*, 81(7), 1537–1575, doi:10.1175/1520-0477(2000)081<1537:BHITAB>2.3.CO;2, 2000.
- Fuentes, J. D., Wang, D., Bowling, D. R., Potosnak, M., Monson, R. K., Goliff, W. S. and Stockwell, W. R.: Biogenic hydrocarbon chemistry within and above a mixed deciduous forest, *J. Atmos. Chem.*, 56(2), 165–185, doi:10.1007/s10874-700 006-9048-4, 2007.
- Gardner, A., Ellsworth, D. S., Crous, K. Y., Pritchard, J. and MacKenzie, A. R.: Is photosynthetic enhancement sustained through three years of elevated CO<sub>2</sub> exposure in 175-year old *Quercus robur*?, *Tree Physiol.*, tpab090, doi:https://doi.org/10.1093/treephys/tpab090, 2021.
- Gerken, T., Chamecki, M. and Fuentes, J. D.: Air-Parcel Residence Times Within Forest Canopies, *Boundary-Layer Meteorol.*, 705 165(1), 29–54, doi:10.1007/s10546-017-0269-7, 2017.
- Gon Seo, Y. and Kook Lee, W.: Single-eddy model for random surface renewal, *Chem. Eng. Sci.*, 43(6), 1395–1402, doi:10.1016/0009-2509(88)85112-1, 1988.
- Guenther, A. B., Jiang, X., Heald, C. L., Sakulyanontvittaya, T., Duhl, T., Emmons, L. K. and Wang, X.: The model of emissions of gases and aerosols from nature version 2.1 (MEGAN2.1): An extended and updated framework for modeling biogenic emissions, *Geosci. Model Dev.*, 5(6), 1471–1492, doi:10.5194/gmd-5-1471-2012, 2012.
- 710 Haghghi, E. and Or, D.: Evaporation from porous surfaces into turbulent airflows: Coupling eddy characteristics with pore scale vapor diffusion, *Water Resour. Res.*, 49(12), 8432–8442, doi:10.1002/2012WR013324, 2013.
- Haghghi, E. and Or, D.: Thermal signatures of turbulent airflows interacting with evaporating thin porous surfaces, *Int. J. Heat Mass Transf.*, 87, 429–446, doi:10.1016/j.ijheatmasstransfer.2015.04.026, 2015.
- 715 Hakola, H., Hellén, H., Hemmilä, M., Rinne, J. and Kulmala, M.: In situ measurements of volatile organic compounds in a boreal forest, *Atmos. Chem. Phys.*, 12(23), 11665–11678, doi:10.5194/acp-12-11665-2012, 2012.
- Hart, K. M., Curioni, G., Blaen, P., Harper, N. J., Miles, P., Lewin, K. F., Nagy, J., Bannister, E. J., Cai, X., Thomas, R. M., Krause, S., Tausz, M. and MacKenzie, A. R.: Characteristics of free air carbon dioxide enrichment of a northern temperate mature forest, *Glob. Chang. Biol.*, 26(2), 1023–1037, doi:10.1111/gcb.14786, 2020.
- 720 Haverd, V., Leuning, R., Griffith, D., van Gorsel, E. and Cuntz, M.: The turbulent lagrangian time scale in forest canopies



- constrained by fluxes, concentrations and source distributions, *Boundary-Layer Meteorol.*, 130(2), 209–228, doi:10.1007/s10546-008-9344-4, 2009.
- von Hippel, P. T.: Mean, median, and skew: Correcting a textbook rule, *J. Stat. Educ.*, 13(2), doi:10.1080/10691898.2005.11910556, 2005.
- 725 Kaimal, J. C. and Gaynor, J. E.: Another look at sonic thermometry, *Boundary-Layer Meteorol.*, 56(4), 401–410, doi:10.1007/BF00119215, 1991.
- Katul, G. and Liu, H.: Evaporation Into a Turbulent Atmosphere, *Water*, 53, 3635–3644, doi:10.1002/2016WR020006.Received, 2017.
- Katul, G., Hsieh, C. I., Oren, R., Ellsworth, D. S. and Phillips, N.: Latent and sensible heat flux predictions from a uniform  
730 pine forest using surface renewal and flux variance methods, *Boundary-Layer Meteorol.*, 80(3), 249–282, doi:10.1007/bf00119545, 1996.
- Katul, G. G., Cava, D., Siqueira, M. and Poggi, D.: Scalar Turbulence within the Canopy Sublayer, edited by J. G. Venditti, J. L. Best, M. Church, and R. J. Hardy, *Coherent Flow Struct. Earth's Surf.*, 73–95, doi:10.1002/9781118527221.ch6, 2013.
- Kesselmeier, J. and Staudt, M.: Biogenic Volatile Organic Compounds (VOC): An Overview on Emission, Physiology and  
735 Ecology, *J. Atmos. Chem.*, 33, 23–88 [online] Available from: [https://link.springer-com.ez27.periodicos.capes.gov.br/content/pdf/10.1023%2FA%3A1006127516791.pdf](https://link.springer.com.ez27.periodicos.capes.gov.br/content/pdf/10.1023%2FA%3A1006127516791.pdf), 1999.
- Larcher, W.: *Physiological Plant Ecology*, Third., Springer-Verlag, Berlin., 1995.
- Lau, G. E., Ngan, K. and Hon, K. K.: Residence times of airborne pollutants in the urban environment, *Urban Clim.*, 34(September), 100711, doi:10.1016/j.uclim.2020.100711, 2020.
- 740 Lin, M., Hang, J., Li, Y., Luo, Z. and Sandberg, M.: Quantitative ventilation assessments of idealized urban canopy layers with various urban layouts and the same building packing density, *Build. Environ.*, 79, 152–167, doi:10.1016/j.buildenv.2014.05.008, 2014.
- Lo, K. W. and Ngan, K.: Characterizing ventilation and exposure in street canyons using Lagrangian particles, *J. Appl. Meteorol. Climatol.*, 56(5), 1177–1194, doi:10.1175/JAMC-D-16-0168.1, 2017.
- 745 MacKenzie, A. R., Langford, B., Pugh, T. A. M., Robinson, N., Misztal, P. K., Heard, D. E., Lee, J. D., Lewis, A. C., Jones, C. E., Hopkins, J. R., Phillips, G., Monks, P. S., Karunaharan, A., Hornsby, K. E., Nicolas-Perea, V., Coe, H., Gabey, A. M., Gallagher, M. W., Whalley, L. K., Edwards, P. M., Evans, M. J., Stone, D., Ingham, T., Commane, R., Furneaux, K. L., McQuaid, J. B., Nemitz, E., Seng, Y., Fowler, D., Pyle, J. A. and Hewitt, C. N.: The atmospheric chemistry of trace gases and particulate matter emitted by different land uses in Borneo, *Philos. Trans. R. Soc. B Biol. Sci.*, 366(1582), 3177–3195,  
750 doi:10.1098/rstb.2011.0053, 2011.
- MacKenzie, A. R., Krause, S., Hart, K. M., Thomas, R. M., Blaen, P. J., Hamilton, R. L., Curioni, G., Quick, S. E., Kourmouli, A., Hannah, D. M., Comer-Warner, S. A., Brekenfeld, N., Ullah, S. and Press, M. C.: BIFoR FACE: Water–soil–vegetation–atmosphere data from a temperate deciduous forest catchment, including under elevated CO<sub>2</sub>, *Hydrol. Process.*, 35(3), 1–8, doi:10.1002/hyp.14096, 2021.
- 755 Mahrt, L.: Stably stratified atmospheric boundary layers, *Annu. Rev. Fluid Mech.*, 46(July), 23–45, doi:10.1146/annurev-fluid-010313-141354, 2014.
- Mahrt, L.: Microfronts in the nocturnal boundary layer, *Q. J. R. Meteorol. Soc.*, 145(719), 546–562, doi:10.1002/qj.3451, 2019.



- Mahrt, L., Sun, J., Blumen, W., Delany, T. and Oncley, S.: Nocturnal boundary-layer regimes, *Boundary-Layer Meteorol.*, 760 88(2), 255–278, doi:10.1023/A:1001171313493, 1998.
- Martens, C. S., Shay, T. J., Mendlovitz, H. P., Matross, D. M., Saleska, S. R., Wofsy, S. C., Woodward, W. S., Menton, M. C., De Moura, J. M. S., Crill, P. M., De Moraes, O. L. L. and Lima, R. L.: Radon fluxes in tropical forest ecosystems of Brazilian Amazonia: Night-time CO<sub>2</sub> net ecosystem exchange derived from radon and eddy covariance methods, *Glob. Chang. Biol.*, 10(5), 618–629, doi:10.1111/j.1365-2486.2004.00764.x, 2004.
- 765 Monin, A. S. and Obukhov, A. M.: Basic laws of turbulent mixing in the surface layer of the atmosphere, *Akad. Nauk SSSR Geofiz. Inst. Tr.*, 24(151), 163–187, 1954.
- Monteith, J. L. and Unsworth, M. H.: *Principles of Environmental Physics*, Fourth., Academic Press, Oxford. [online] Available from: <http://elsevier.com/locate/permissions>, (Accessed 11 February 2020), 2008.
- Patton, E. G., Sullivan, P. P., Shaw, R. H., Finnigan, J. J. and Weil, J. C.: Atmospheric stability influences on coupled boundary layer and canopy turbulence, *J. Atmos. Sci.*, 73(4), 1621–1647, doi:10.1175/JAS-D-15-0068.1, 2016.
- 770 Paw U, K. T., Qiu, J., Su, Hong-bing, Watanabe, T. and Brunet, Y.: Surface renewal analysis: a new method to obtain scalar fluxes, *Agric. For. Meteorol.*, 74, 119–137 [online] Available from: [papers3://publication/uuid/0E2DD6E8-90ED-442D-8B50-8B9E69DA8647](https://papers3://publication/uuid/0E2DD6E8-90ED-442D-8B50-8B9E69DA8647), 1995.
- Peñuelas, J. and Staudt, M.: BVOCs and global change, *Trends Plant Sci.*, 15(3), 133–144, doi:10.1016/j.tplants.2009.12.005, 775 2010.
- Pyle, J. A., Warwick, N. J., Harris, N. R. P., Abas, M. R., Archibald, A. T., Ashfold, M. J., Ashworth, K., Barkley, M. P., Carver, G. D., Chance, K., Dorsey, J. R., Fowler, D., Gonzi, S., Gostlow, B., Hewitt, C. N., Kurosu, T. P., Lee, J. D., Langford, S. B., Mills, G., Moller, S., MacKenzie, A. R., Manning, A. J., Misztal, P., Nadzir, M. S. M., Nemitz, E., Newton, H. M., O'Brien, L. M., Ong, S., Oram, D., Palmer, P. I., Peng, L. K., Phang, S. M., Pike, R., Pugh, T. A. M., Rahman, N. A., Robinson, 780 A. D., Sentian, J., Samah, A. A., Skiba, U., Ung, H. E., Yong, S. E. and Young, P. J.: The impact of local surface changes in Borneo on atmospheric composition at wider spatial scales: Coastal processes, land-use change and air quality, *Philos. Trans. R. Soc. B Biol. Sci.*, 366(1582), 3210–3224, doi:10.1098/rstb.2011.0060, 2011.
- R Core Team: R: A language and environment for statistical computing, [online] Available from: <https://www.r-project.org/>, 2021.
- 785 Rap, A., Scott, C. E., Reddington, C. L., Mercado, L., Ellis, R. J., Garraway, S., Evans, M. J., Beerling, D. J., MacKenzie, A. R., Hewitt, C. N. and Spracklen, D. V.: Enhanced global primary production by biogenic aerosol via diffuse radiation fertilization, *Nat. Geosci.*, 11(9), 640–644, doi:10.1038/s41561-018-0208-3, 2018.
- Raupach, M. R.: Applying Lagrangian fluid mechanics to infer scalar source distributions from concentration profiles in plant canopies, *Agric. For. Meteorol.*, 47(2–4), 85–108, doi:10.1016/0168-1923(89)90089-0, 1989.
- 790 Raupach, M. R., Finnigan, J. J. and Brunet, Y.: Coherent Eddies and Turbulence in Vegetation Canopies: The Mixing-Layer Analogy, *Boundary-Layer Meteorol. 25th Anniv. Vol. 1970–1995*, 351–382, doi:10.1007/978-94-017-0944-6\_15, 1996.
- Rummel, U.: Turbulent exchange of ozone and nitrogen oxides between an amazonian rain forest and the atmosphere, University of Bayreuth., 2005.
- Rummel, U., Ammann, C. and Meixner, F. X.: Characterizing turbulent trace gas exchange above a dense tropical rain forest using wavelet and surface renewal analysis, 15th AMS Symp. *Bound. Layers Turbul.*, (1), 602–605, 2002.
- 795 Schmidt, M., Jochheim, H., Kersebaum, K. C., Lischeid, G. and Nendel, C.: Gradients of microclimate, carbon and nitrogen



- in transition zones of fragmented landscapes – a review, *Agric. For. Meteorol.*, 232, 659–671, doi:10.1016/j.agrformet.2016.10.022, 2017.
- Simon, E., Lehmann, B. E., Ammann, C., Ganzeveld, L., Rummel, U., Meixner, F. X., Nobre, A. D., Araújo, A. and  
800 Kesselmeier, J.: Lagrangian dispersion of <sup>222</sup>Rn, H<sub>2</sub>O and CO<sub>2</sub> within Amazonian rain forest, *Agric. For. Meteorol.*, 132(3–4), 286–304, doi:10.1016/j.agrformet.2005.08.004, 2005.
- Sterk, H. A. M., Steeneveld, G. J., Bosveld, F. C., Vihma, T., Anderson, P. S. and Holtslag, A. A. M.: Clear-sky stable boundary layers with low winds over snow-covered surfaces. Part 2: Process sensitivity, *Q. J. R. Meteorol. Soc.*, 142(695), 821–835, doi:10.1002/qj.2684, 2016.
- 805 Strong, C., Fuentes, J. D. and Baldocchi, D. D.: Reactive hydrocarbon flux footprints during canopy senescence, *Agric. For. Meteorol.*, 127(3–4), 159–173, doi:10.1016/j.agrformet.2004.07.011, 2004.
- Toomey, M., Friedl, M. A., Frohling, S., Hufkens, K., Klosterman, S., Sonnentag, O., Baldocchi, D. D., Bernacchi, C. J., Biraud, S. C., Bohrer, G., Brzostek, E., Burns, S. P., Coursolle, C., Hollinger, D. Y., Margolis, H. A., McCaughey, H., Monson, R. K., Munger, J. W., Pallardy, S., Phillips, R. P., Torn, M. S., Wharton, S., Zeri, M. and Richardson, A. D.: Greenness indices  
810 from digital cameras predict the timing and seasonal dynamics of canopy-scale photosynthesis, *Ecol. Appl.*, 25(1), 99–115, doi:10.1890/14-0005.1, 2015.
- Trumbore, S., Keller, M., Wofsy, S. C. and Da Costa, J. M.: Measurements of Soil and Canopy Exchange Rates in the Amazon Rain Forest using <sup>222</sup>Rn, *J. Geophys. Res.*, 95(D10), 16865–16873, doi:https://doi.org/10.1029/JD095iD10p16865, 1990.
- Wharton, S., Ma, S., Baldocchi, D. D., Falk, M., Newman, J. F., Osuna, J. L. and Bible, K.: Influence of regional nighttime  
815 atmospheric regimes on canopy turbulence and gradients at a closed and open forest in mountain-valley terrain, *Agric. For. Meteorol.*, 237–238, 18–29, doi:10.1016/j.agrformet.2017.01.020, 2017.
- Woebbecke, D. M., Meyer, G. E., Von Bargaen, K. and Mortensen, D. A.: Color indices for weed identification under various soil, residue, and lighting conditions, *Trans. Am. Soc. Agric. Eng.*, 38(1), 259–269, doi:10.13031/2013.27838, 1995.
- Wolfe, G. M., Thornton, J. A., McKay, M. and Goldstein, A.: Forest-atmosphere exchange of ozone: sensitivity to very reactive  
820 biogenic VOC emissions and implications for in-canopy photochemistry, *Atmos. Chem. Phys.*, 11, 7875–7891, doi:10.5194/acp-11-7875-2011, 2011.
- Yaglom, M.: Similarity laws for constant-pressure and pressure-gradient turbulent wall flows, *Annu. Rev. Fluid Mech.*, 11, 505–540, 1979.
- Yan, G., Hu, R., Luo, J., Weiss, M., Jiang, H., Mu, X., Xie, D. and Zhang, W.: Review of indirect optical measurements of  
825 leaf area index: Recent advances, challenges, and perspectives, *Agric. For. Meteorol.*, 265(October 2018), 390–411, doi:10.1016/j.agrformet.2018.11.033, 2019.
- Zorzetto, E., Peltola, O., Grönholm, T. and Katul, G. G.: Intermittent Surface Renewals and Methane Hotspots in Natural Peatlands, *Boundary-Layer Meteorol.*, 180(3), 407–433, doi:10.1007/s10546-021-00637-x, 2021.